AD-759 499

TWO-STAGE HIGH PRESSURE-RATIO CENTRIFUGAL COMPRESSOR

Colin Rodgers

Solar

Prepared for:

Army Air Mobility Research and Development Laboratory

March 1973

AD

AD 759499

USAAMRDL TECHNICAL REPORT 73-4

TWO-STAGE HIGH PRESSURE-RATIO CENTRIFUGAL COMPRESSOR

By

Colin Rodgers

March 1973

EUSTIS DIRECTORATE
U. S. ARMY AIR MOBILITY RESEARCH AND DEVELOPMENT LABORATORY
FORT EUSTIS, VIRGINIA

CONTRACT DAAJ02-72-C-0014
SOLAR DIVISION OF INTERNATIONAL HARVESTER COMPANY
SAN DIEGO, CALIFORNIA

65

DISCLAIMERS

The findings in this report are not to be construed as an official Department of the Army position unless so designated by other authorized documents.

When Government drawings, specifications, or other data are used for any purpose other than in connection with a definitely related Government procurement operation, the United States Government thereby incurs no responsibility nor any obligation whatsoever; and the fact that the Government may have formulated, furnished, or in any way supplied the said drawings, specifications, or other data is not to be regarded by implication or otherwise as in any manner licensing the holder or any other person or corporation, or conveying any rights or permission, to manufacture, use, or sell any patented invention that may in any way be related thereto.

Trade names cited in this report do not constitute an official endorsement or approval of the use of such commercial hardware or software.

DISPOSITION INSTRUCTIONS

Destroy this report when no longer needed. Do not return it to the originator.

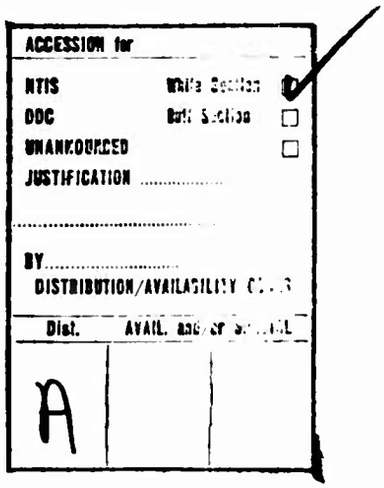

DEPARTMENT OF THE ARMY
U. S. ARMY AIR MOBILITY RESEARCH & DEVELOPMENT LABORATORY
EUSTIS DIRECTORATE
FORT EUSTIS, VIRGINIA 23604

The objective of this contractual effort was to demonstrate that two existing centrifugal compressor stages could be scaled, matched, and run on the same shaft to provide aerodynamic performance comparable to that achievable using state-of-the-art axial centrifugal compressor technology. The target performance was to be demonstrated without benefit of compressor variable geometry, using existing impeller tooling and hot turbine drive design.

This report was prepared by the Solar Division of International Harvester Company under the terms of Contract DAAJ02-72-C-0014. It presents the aeromechanical design of the compressor, test results, and an analysis of these results. An analysis of mechanical problems encountered and recommendations for additional research are also presented.

This report has been reviewed by the technical personnel of this Directorate. The conclusions contained herein are concurred in by this Directorate and will be considered in any future centrifugal compressor programs. The U.S. Army project engineer for this effort was Mr. Robert A. Langworthy, Technology Applications Division.

Task 1G162207AA7102
Contract DAAJ02-72-C-0014
USAAMRDL Technical Report 73-4
March 1973

TWO-STAGE HIGH-PRESSURE-RATIO CENTRIFUGAL COMPRESSOR

Final Technical, Test, and Demonstration Report

Solar ER 2415

By

Colin Rodgers

Prepared by

Solar Division of International Harvester Company
San Diego, California

for

EUSTIS DIRECTORATE
U.S. ARMY AIR MOBILITY RESEARCH AND DEVELOPMENT LABORATORY
FORT EUSTIS, VIRGINIA

Unclassified
Security Classification

DOCUMENT CONTROL DATA - R & D

(Security classification of title, body of abstract and indexing annotation must be entered when the overall report is classified)

1. ORIGINATING ACTIVITY (Corporate author) Solar, Division of International Harvester Company 2200 Pacific Highway San Diego, California	2a. REPORT SECURITY CLASSIFICATION Unclassified 2b. GROUP N/A

3. REPORT TITLE

TWO-STAGE HIGH-PRESSURE-RATIO CENTRIFUGAL COMPRESSOR

4. DESCRIPTIVE NOTES (Type of report and inclusive dates)

Final Techanical, Test, and Demonstration Report

5. AUTHOR(S) (First name, middle initial, last name)

Colin (NMI) Rodgers

6. REPORT DATE	7a. TOTAL NO. OF PAGES	7b. NO. OF REFS
March 1973	65	

8a. CONTRACT OR GRANT NO.	9a. ORIGINATOR'S REPORT NUMBER(S)
DAAJ02-72-C-0014	
b. PROJECT NO. Task 1G162207AA7102	USAAMRDL Technical Report 73-4
c.	9b. OTHER REPORT NO(S) (Any other numbers that may be assigned this report) ER 2415
d.	

10. DISTRIBUTION STATEMENT

Approved for public release; distribution unlimited.

11. SUPPLEMENTARY NOTES	12. SPONSORING MILITARY ACTIVITY
	Eustis Directorate U.S. Army Air Mobility Research and Development Laboratory Fort Eustis, Virginia

13. ABSTRACT

This report presents the aerodynamic design parameters along with the overall and stage test performances of a small, advanced, two-stage centrifugal compressor designed to attain high pressure ratios with fixed geometry. Complete performance test data was obtained at 60, 70, 80, 90, and 95 percent design speed, showing peak overall temperature rise adiabatic efficiencies of up to 80.5 percent, at pressure ratios between 3.4 and 11.2. Although several data points were recorded at 100 percent speed, only two were probably representative of valid performance potential with the proper first-stage shroud clearance. The highest pressure ratio was 12.3 with an overall adiabatic efficiency of 78.3 percent. Broad compressor flow ranges between surge and choke flows were exhibited, substantiating design predictions that operation at high pressure ratios could be obtained on a two-stage centrifugal compressor without the necessity for variable geometry.

DD FORM 1 NOV 68 1473 REPLACES DD FORM 1473, 1 JAN 64, WHICH IS OBSOLETE FOR ARMY USE.

Unclassified
Security Classification

14. KEY WORDS	LINK A		LINK B		LINK C	
	ROLE	WT	ROLE	WT	ROLE	WT
Compressors Compressors, Centrifugal, Engine Efficiency, Engines, Gas Turbine						

SUMMARY

This report presents the aerodynamic design parameters and the overall and stage test performances of a small, advanced, two-stage centrifugal compressor designed to attain high pressure ratios with fixed geometry.

Complete performance test data was obtained at 60, 70, 80, 90, and 95 percent of design speed, showing peak overall temperature rise adiabatic efficiencies of up to 80.5 percent, at pressure ratios between 3.4 and 11.2.

A compressor discharge scroll casing distortion problem at 100 percent speed (82,000 rpm) was experienced, resulting in a progressive increase in first-stage impeller operating clearance.

Although several data points were recorded at 100 percent speed, only two were probably representative of valid performance potential with the proper first-stage shroud clearance. The highest pressure ratio was 12.3 with a corresponding overall adiabatic efficiency of 78.3 percent.

Broad compressor flow ranges between surge and choke flows were exhibited, substantiating design predictions that operation at high pressure ratios could be obtained on a two-stage centrifugal compressor without the necessity for variable geometry.

It is recommended that the discharge scroll design be modified to solve the shroud distortion problem and to enable subsequent completion of performance testing with the current component matching, followed by an additional test with a possible diffuser rematching.

FOREWORD

This technical report covers all design and experimental work necessary to fulfill the requirements of Contract DAAJ02-72-C-0014, DA Task 1G162207AA7102, with the Eustis Directorate, U.S. Army Air Mobility Research and Development Laboratory, Fort Eustis, Virginia.

The technical representative of the U.S. Army was Mr. R.A. Langworthy of the Eustis Directorate.

The principal investigator responsible for the technical content, execution, and liaison of the program was C. Rodgers. Other Solar personnel engaged in the program included J. Thayer, Experimental Engineer; M. Lafferty, Design Engineer; and P. Carlson, Program Manager.

TABLE OF CONTENTS

LIST OF ILLUSTRATIONS

LIST OF ILLUSTRATIONS - Continued

LIST OF TABLES

LIST OF SYMBOLS

A	Area, $in.^2$
b	Blade height, in.
C	Absolute velocity, ft/sec
CF	Skin friction coefficient
cfs	Inlet volume flow based on stagnation pressure, ft^3/sec
Cp	Specific heat at constant pressure, 0.243 Btu/lb°R for air
CP	Diffuser static pressure recovery = $\frac{\text{Static pressure rise}}{\text{Inlet dynamic head}}$
D	Diameter, in.
DF	Diffusion factor
DP	Design point
E	Exit
F	Axial thrust, lb
g	Gravitational constant, 32.2 ft/sec^2
H_{ad}	Adiabatic head, $JC_p \Delta T_{ad}$ ft
J	Joules equivalent of heat, 778 ft-lb/Btu
K	Constant for axial thrust calculation
KSI	Thousands, $lb/in.^2$
L	Impeller blade flow path length, in.
M	Mach number
N	Rotational speed, rpm
NS	Specific speed, $rpm \cdot cfs^{0.5} \cdot H_{ad}{}^{-0.75}$
P	Pressure, $lb/in.^2$
q	Work factor, $gJCp\Delta T/U_2{}^2$
RMS	Root mean square
RHO	Density, lb/ft^3
RWD	Diffuser relative flow parameter, $\frac{W\sqrt{T_3}}{A_3 P_3} / \frac{W\sqrt{T_3}}{A\ P_3}$ $(M_3 = 1.0)$
S	Static flow conditions (also STA)
T	Temperature °F, °R, or stagnation flow conditions (also TOT)

U	Blade tip speed, ft/sec
uts	Ultimate tensile strength, $lb/in.^2$
W	Airflow, lb/sec; also
	Relative velocity, ft/sec
Z	Impeller blade number
α	Air angle (relative to axial direction), deg
β	Blade angle (relative to axial direction), deg
γ	Specific heat ratio, 1.395
Δ	Difference
δ	Inlet relative pressure, psia/14.7
η	Efficiency (ETA), based on temperature rise
θ	Inlet prewhirl (THETA); also $\frac{\text{Inlet temperature °R}}{519}$
λ	Blockage fraction, $\frac{\text{Effective area}}{\text{Geometrical area}}$ (LAM)
ω	Impeller pressure loss coefficient

SUBSCRIPTS

1	Impeller inlet
2	Impeller tip
3	Vaned diffuser throat
4	Vaned diffuser exit
C	Compressor
E	Exit
H	Inducer hub
S	Inducer shroud
ad	Adiabatic

INTRODUCTION

Extensive studies of various methods of obtaining pressure ratios between 10 and 20:1, with airflows ranging from 2.0 to 5.0 pounds per second (pps), for advanced, small, low-cost gas turbines were conducted at Solar during the period 1969-1971. Three basic compressor configurations were examined:

- Single-stage axial transonic plus single-stage centrifugal
- Two-stage axial transonic plus single-stage centrifugal
- Two-stage centrifugal

The results of these studies indicated that up to overall pressure ratios of 14.0:1, the two-stage centrifugal compressor configuration could probably provide equal performance to the two-stage axial transonic plus centrifugal stage, and probably would not require variable geometry to obtain adequate surge margin for advanced gas turbine application.

Preliminary matching studies were conducted for a two-stage centrifugal-compressor configuration, using as a baseline individual stage characteristics for existing high- and low-specific-speed compressor designs developed at Solar in 1970. Matching analysis showed that it should be possible to obtain an overall compressor efficiency of 79 percent, at 14.0:1 pressure ratio, with an airflow of 2.0 pps and a rotational speed of 82,000 rpm, with components scaled from existing 1970 designs.

As the result of an unsolicited approach to the Eustis Directorate, USAAMRDL, a compressor research program was procured to design, fabricate, and test such a two-stage centrifugal compressor. The compressor design approach, test procedures and performance, and the results of various analytical studies performed are presented in this report.

DISCUSSION OF WORK PERFORMED

AERODYNAMIC DESIGN

The two-stage centrifugal compressor was designed for the following overall performance:

Pressure ratio	14.0 (total - total)
Inlet corrected airflow, lb/sec	2.05
Rotational speed, rpm	82,000
Overall adiabatic efficiency, percent	79 (total - total)

This level of performance was to be obtained by using first- and second-stage compressor designs scaled from existing baseline high- and low-specific-speed compressor types previously developed at Solar. The only new aerodynamic component required, the interstage crossover, was designed with turning vanes to reduce the entry swirl to the second-stage impeller to 7.0 degrees with a minimum of total pressure loss. The design of the interstage crossover duct was based upon similarity with existing Solar multi-stage centrifugal compressor crossovers.

The respective scale factors required for each stage to give design point performance were 0.8 and 1.266, with impeller tip diameters of 5.06 and 4.75 inches. The meridional dimensions of the scaled compressors are given in Figure 1. Both impellers from which the two-stage compressor was scaled are typical of the latest generation of small centrifugal compressors which employ 40 degrees of blade backsweep (relative to radial direction) at the tip. Using advanced design techniques coupled with extensive testing, this type of design has consistently exhibited high efficiencies with extended flow range at stage pressure ratios up to 6.0.

The design point aerodynamic details for both stages are listed in Table I. First-stage pressure ratio and specific speed were 4.9 and 116. Second-stage pressure ratio and specific speed were 2.86 and 69.0. Estimated impeller blading velocity distribution plots for each stage are shown in Figure 2.

Nineteen vanes of relatively high solidity were selected for the crossover turning vanes to accomplish an air turning from 63 degrees at the inlet to a residual exit swirl of 7.0 degrees (with rotation). Turning vane diffusion factor was 0.65 with an average absolute Mach number of 0.210.

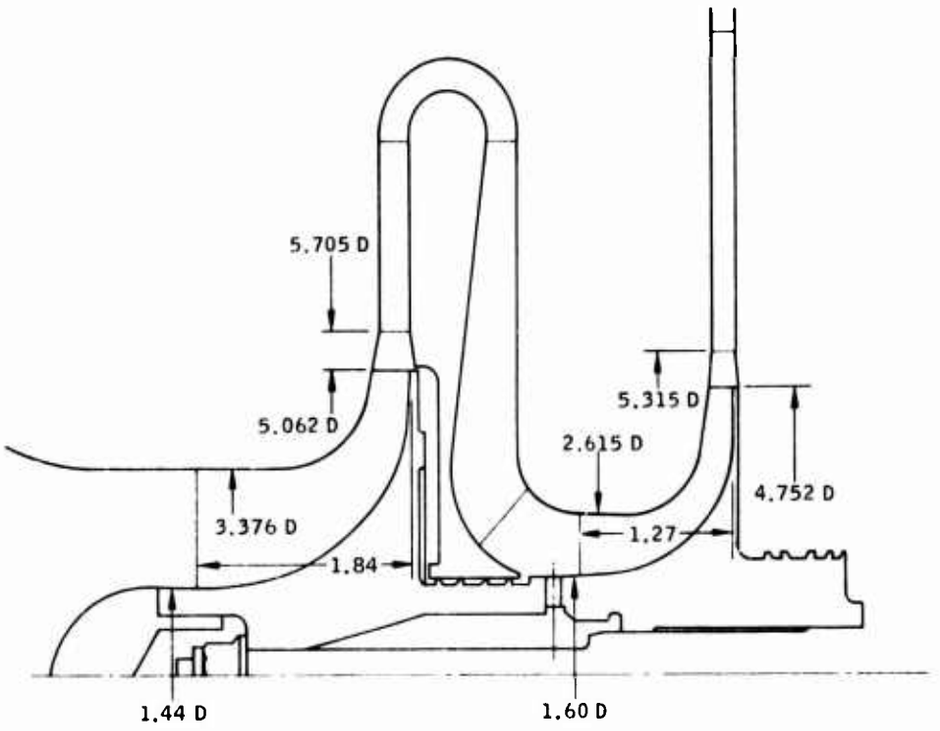

Figure 1. Impeller Dimensions (inches).

The first-stage diffuser vanes were designed with 1.5 percent bleed-air takeoff along the critical suction surface prior to the throat. The slot position and geometry were scaled from a similar-design channel diffuser on an advanced experimental Solar centrifugal compressor. The slot configuration is shown in Figure 3. Slot entry height is 0.009 to 0.011 inch.

MECHANICAL DESIGN

Impeller Stress Analysis

First- and second-stage impeller disc stresses and blade distortions were computed employing a finite-element stress program, and are shown on Figures 4 and 5 respectively. Maximum effective stresses at design speed and material uts limitations are listed below:

STAGE	FIRST	SECOND
Maximum effective stress (hub), KSI	76.4	52.4
Material	Ti6A4V	Ti6242
Ultimate tensile strength, KSI	140	140

TABLE I. TWO-STAGE COMPRESSOR AERODYNAMIC DESIGN PARAMETERS

	1ST STAGE	2ND STAGE
Inlet pressure, $lb/in.^2$	14.7	72.0
Inlet temperature, °F	60	425
Inducer tip diameter, in.	3.376	2.615
Inducer hub diameter, in.	1.44	1.59
Inducer tip Mach number	1.248	0.69
Inducer RMS Mach number	1.027	0.59
Inducer RMS air angle, deg	56.0	59.5
Inducer RMS incidence, deg	+7.0	+9.5
Impeller tip Mach number	0.95	0.78
Impeller tip speed, ft/sec	1810	1700
Impeller tip diameter, in.	5.06	4.75
Impeller tip width, in.	0.296	0.180
Impeller tip air angle, deg	71.2	74.7
Impeller tip blade angle, deg	40.0	40.0
Impeller efficiency, %	86.0	91.0
Diffuser leading edge diameter, in.	5.70	5.32
Diffuser inlet Mach number	0.738	0.605
Diffuser throat/exit area ratio	1.83	2.26
Diffuser throat/length ratio	5.3	9.1
Diffuser exit diameter, in.	8.3	10.6
Diffuser exit Mach number	0.31	0.215
Overall diffuser static recovery	0.79	0.73
Corrected airflow, lb/sec	2.05	0.545
Stage pressure ratio	4.9	2.86
Stage efficiency, %	81.0	83.6
Stage specific speed, $\frac{rpm\sqrt{cfs}}{ft^{3/4}}$	116	69.0
Work factor, q	0.68	0.760

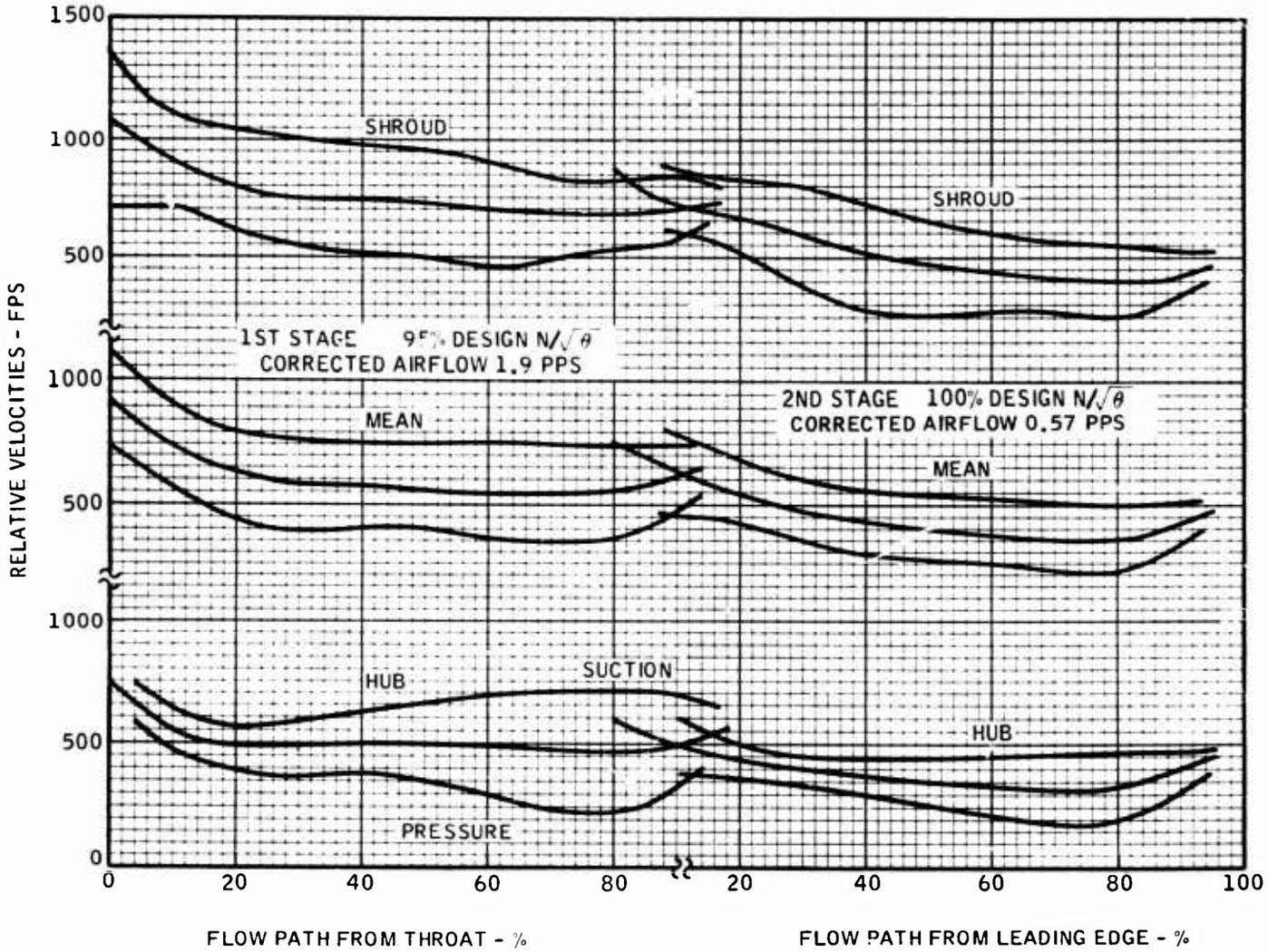

Figure 2. Impeller Velocity Distributions.

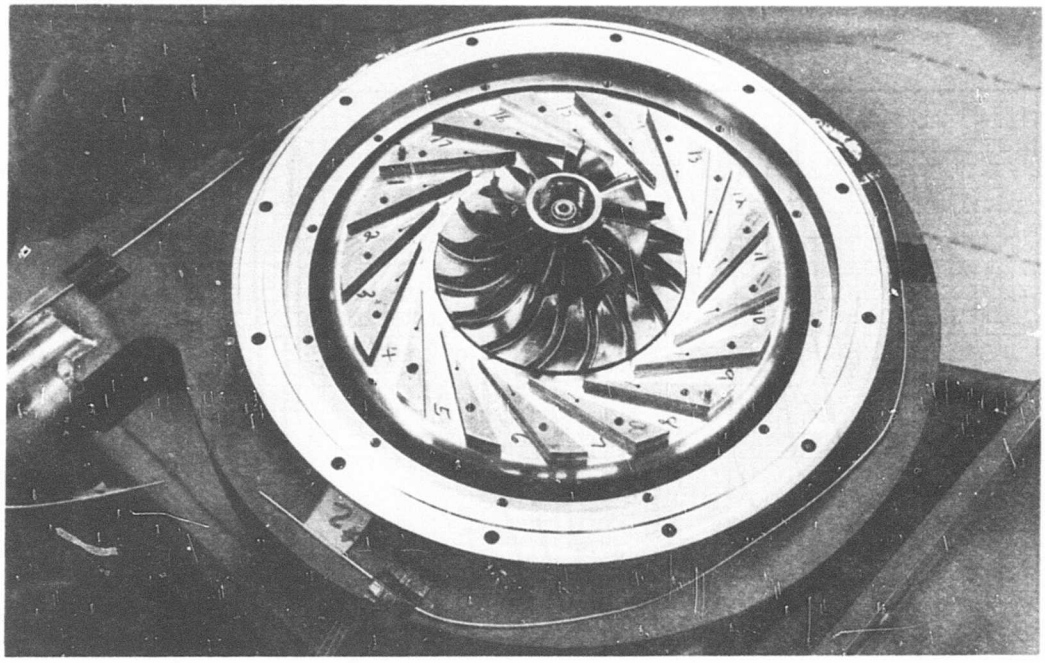

Figure 3. First-Stage Impeller and Diffuser.

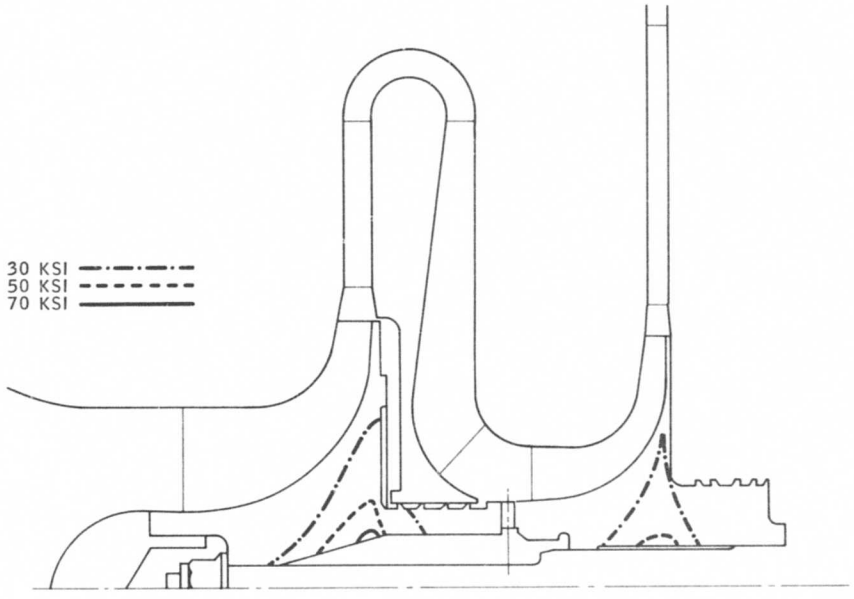

Figure 4. Effective Stress Contours.

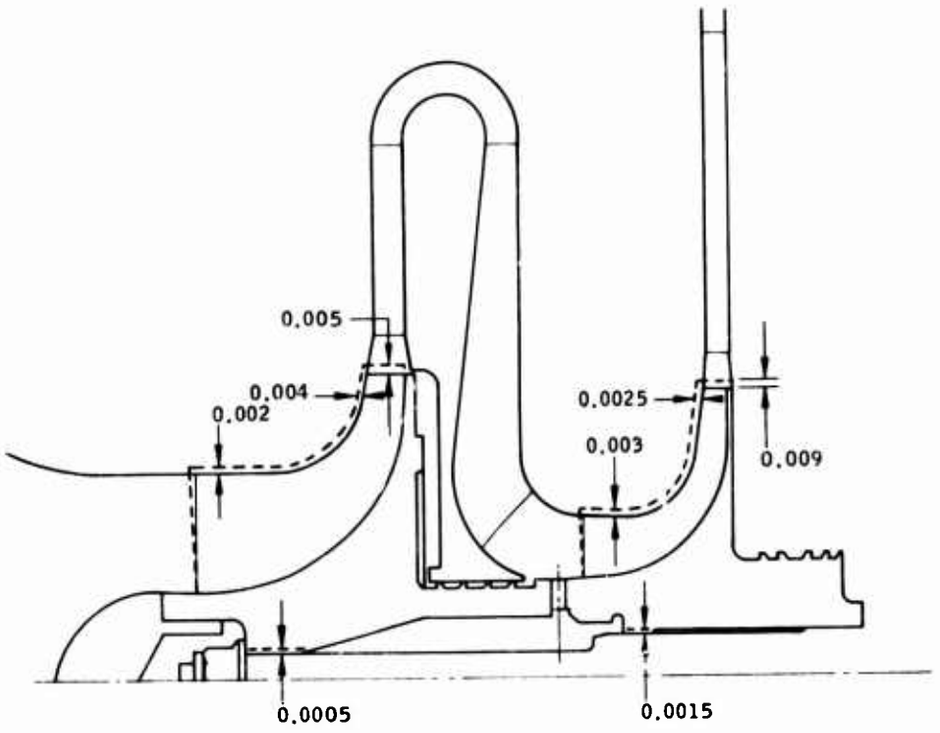

Figure 5. Dynamic Plus Thermal Distortions (inches).

Experimentally determined maximum blade stresses for the baseline first-stage design were 75 KSI in the same material at an equivalent tip speed of 1675 fps. Design tip speed for the scaled first stage was 1810 fps, increasing blade stresses to

$$\left(\frac{1810}{1675}\right)^2 \times 75 = 87 \text{ KSI}$$

Blade stresses were not experimentally determined for the baseline second-stage impeller with the same sweepback, but will be lower than the first stage since the blade heights are relatively smaller with a lower specific speed design.

Impeller Resonance Diagrams

Impeller resonance diagrams for the first and second stages were constructed, based upon vibration shaker table data of the baseline compressors at the first flap mode of the inducer. Figure 6 shows that the first stage is clear of any excitation that may arise from 17-vane diffusers downstream.

The second-stage impeller could possibly be excited by either the 19 vanes of the interstage duct or the 15 vanes of the diffuser downstream between 50 and 65 percent design speed.

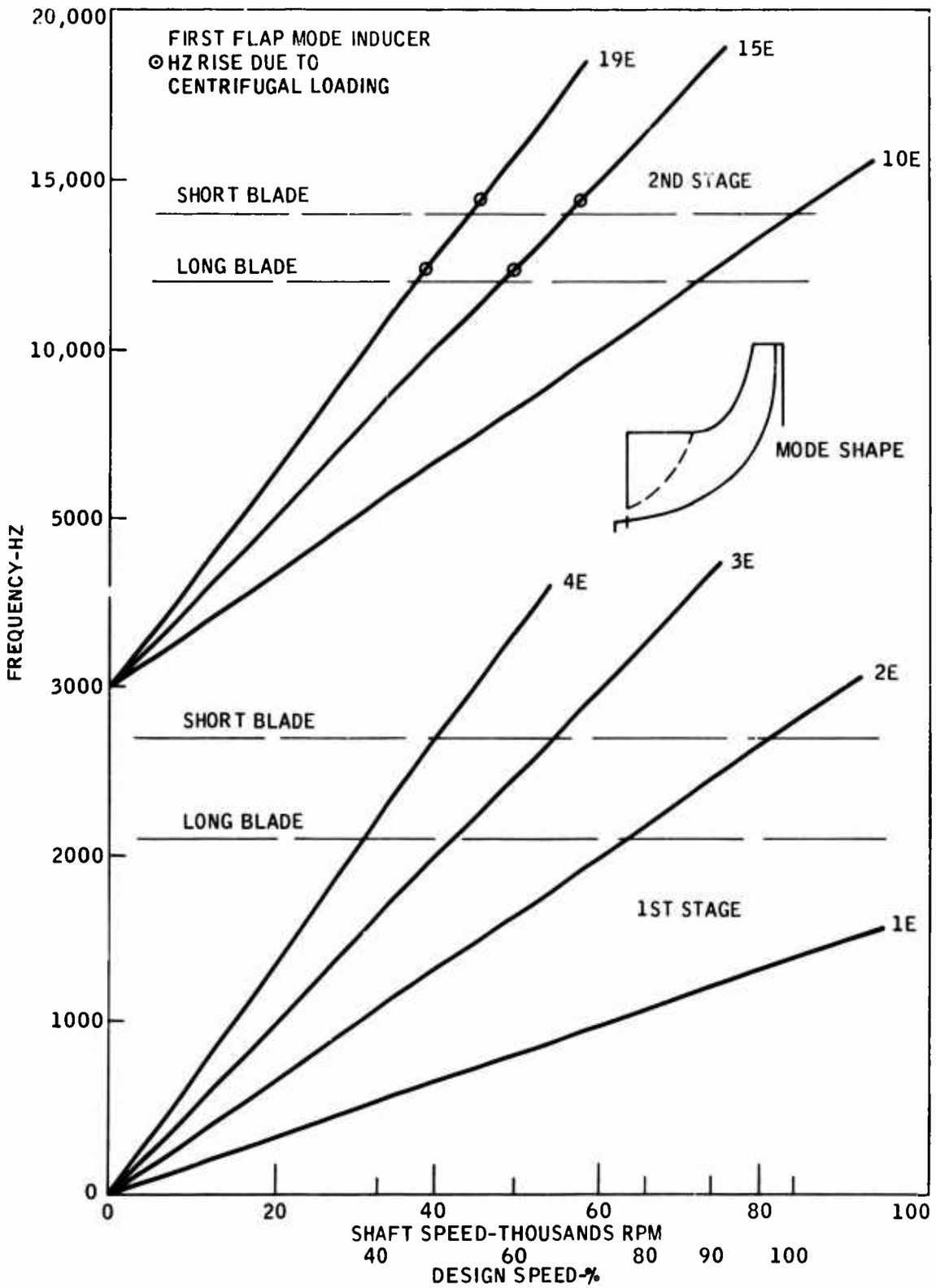

Figure 6. Two-Stage Compressor Rotor Resonance Diagrams.

Bearing and Seal Design

A straddle-mounted compressor and turbine system with the two compressor stages cantilevered from the front bearing was selected after preliminary dynamic calculations had indicated that the amount of overhang was acceptable. This arrangement permits a clean inlet to the first-stage compressor, and simplifies component assembly.

The bearing system for the straddle rotor assembly was similar to one previously developed for a turbodrive rig. Two preloaded angular-contact M204 ball bearings are contained in a capsule which is mounted in the support housing. Estimated B-10 bearing lives are shown as a function of axial end thrust and rotational speed in Figure 7.

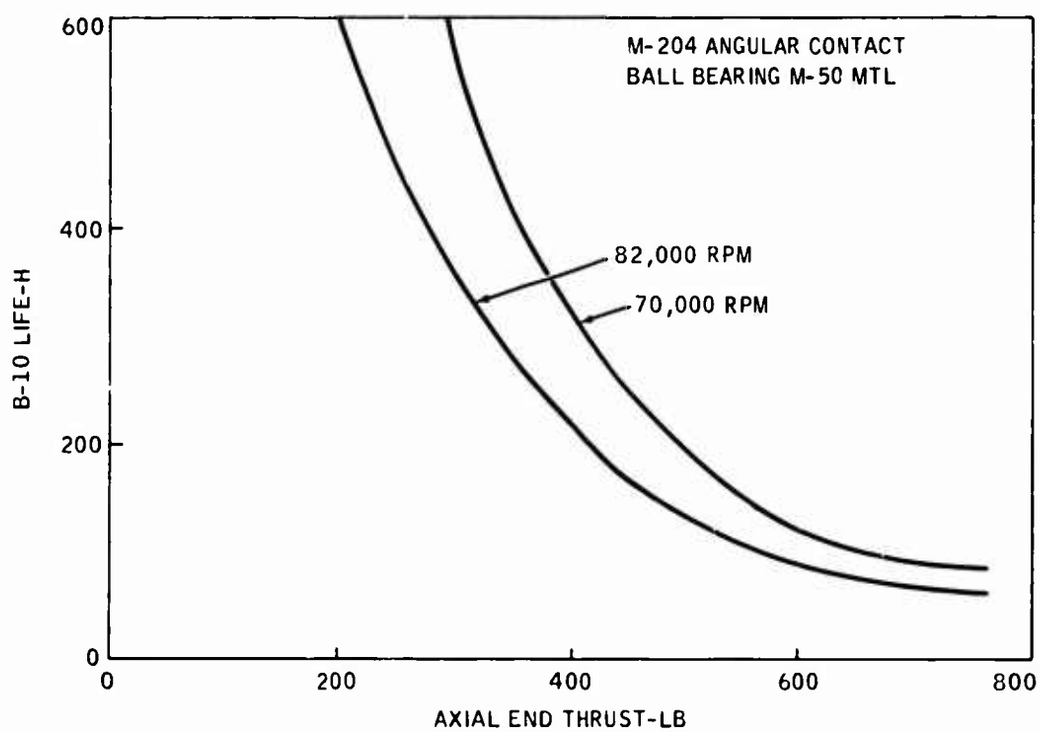

Figure 7. Estimated B-10 Bearing Life.

Six equally spaced, radially bladed pumping blades, 0.060 inch high, were designed for the back shroud of the second-stage impeller to reduce the axial end thrust of the rotating assembly.

With the pumping blades, estimated aerodynamic end thrust was 120 lb, which, together with a spring preload of 275 lb, resulted in a calculated B-10 life at 82,000 rpm of 200 hours. Aerodynamic end thrust was calculated for each compressor operating point during performance evaluation in order to check acceptable operating conditions.

Thermocouples were installed on the bearing outer races and connected to an automatic shutdown device in the event of excessive operating temperatures.

All three aerodynamic seals are of the rub-in labyrinth type, SAE 64 (80/10/10). Bronze was selected for the seal material. The turbine-end oil labyrinth is buffered by shop air. The compressor-end lube oil seal has bleed-down capability, and is further assisted by six blades incorporated in the reverse face of the second-stage impeller. The pressure gradient generated by these blades, besides minimizing aerodynamic thrust loads, serves to reduce the seal pressure differential. The interstage seal is unbuffered.

Rotor Dynamic Response

Two different unbalance distributions were applied along the rotor span, with light damping of 10.0 lb-sec/in. at the two bearing locations. Unbalance loads of 0.003 oz-in. were applied at two planes of each of the three rotors.

Output from the computer dynamic response programs consists of rotor radial excursions along with dynamic bearing loads as a function of speed. Figure 8 shows the response for the in-phase unbalance condition. The criticals appear at 22,000 and 34,000 rpm. The excursions shown represent steady-state running values which would occur if the speed were held constant; values would be much reduced during transient speed operation.

The unbalance response for a couple unbalance in the two compressor rotors is given in Figure 9. The criticals appear as before, but the overall reponse is somewhat lower.

In general, the dynamic response is well behaved, and the excursions indicated no potential problems in the operation of the rig. Unbalance of the final rotor system was held below the assumed values of 0.003 oz-in.; thus, anticipated actual excursions were expected to be correspondingly lower.

COMPRESSOR FABRICATION AND ASSEMBLY

The Solar-designed turbodrive compressor rig, Figure 10, is primarily an aerodynamic research rig with structural design emphasizing compatibility with existing turbodrive test facilites and reasonable cost wherever possible. Apart from the impellers and interstage crossover assembly, the majority of stationary hardware fabrication was straightforward, using weldments and other standard techniques.

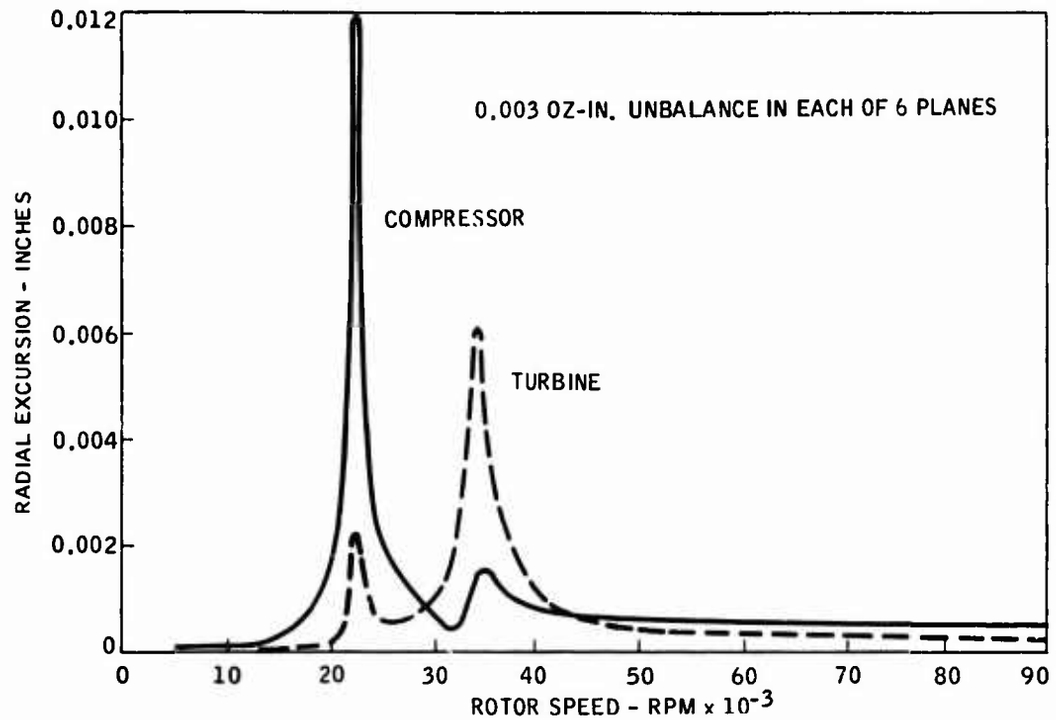

Figure 8. Rig Dynamic Excursions; In-Phase Unbalance.

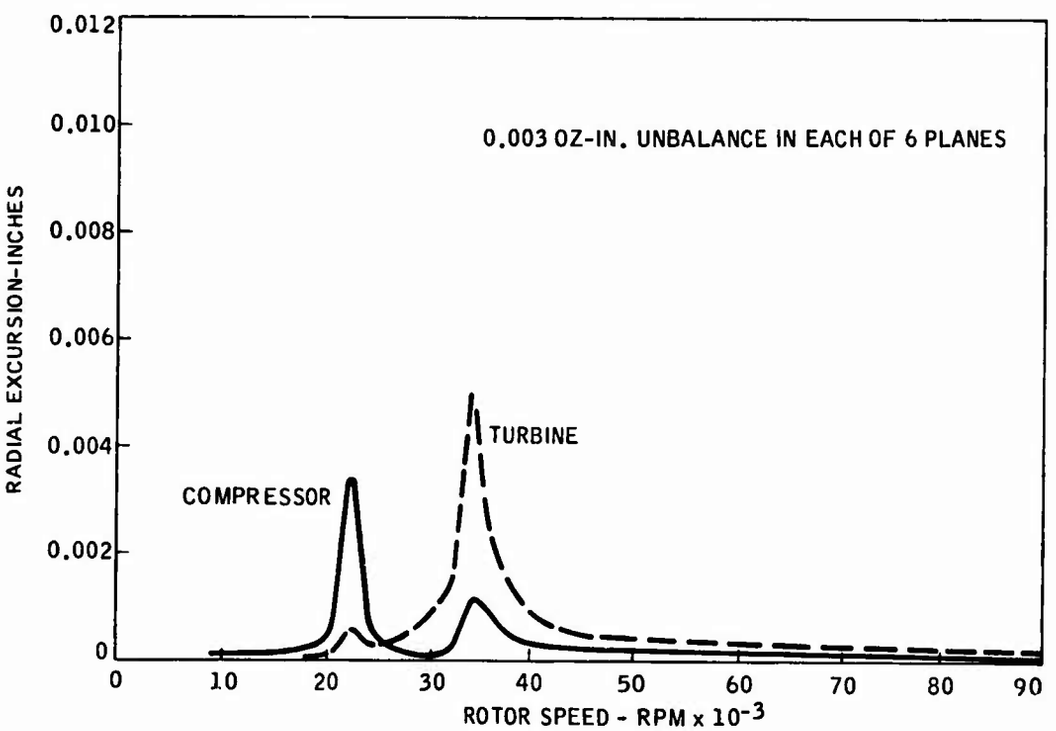

Figure 9. Rig Dynamic Excursions; Out-of-Phase Unbalance.

The test compressor rig incorporates two integrally machined centrifugal compressors mounted in series on a common shaft, driven by a modified Solar Titan radial inward-flow turbine. The rotating assembly is supported by two angular-contact bearings. The bearing capsule is located between the turbine and compressor assembly, thereby facilitating removal of the rotating components without disturbing the bearing capsule. Figure 11 shows the rotating assembly and bearing capsule. The first-stage impeller is located relative to the second-stage impeller by a curvic coupling. This location technique was selected to allow removal and reassembly of the first-stage impeller without the need for rebalancing. Figure 12 shows the two-stage impeller assembly and curvic coupling arrangements. Both compressor impellers and the turbine rotor are interference-mounted on the shaft and axially bolted against the bearing shoulders.

Bleed slots are incorporated in the first-stage diffuser ahead of the throat section to enhance surge characteristics. The first-stage diffuser and interstage crossover turning vanes were integrally machined from a single forging. Figure 13 shows both faces of the interstage crossover and the position of the bleed slots in relation to the diffuser throats. Figure 14 shows the second-stage vaned diffuser with the separate vaned diffuser wedges attached by dowel pins to the front shroud.

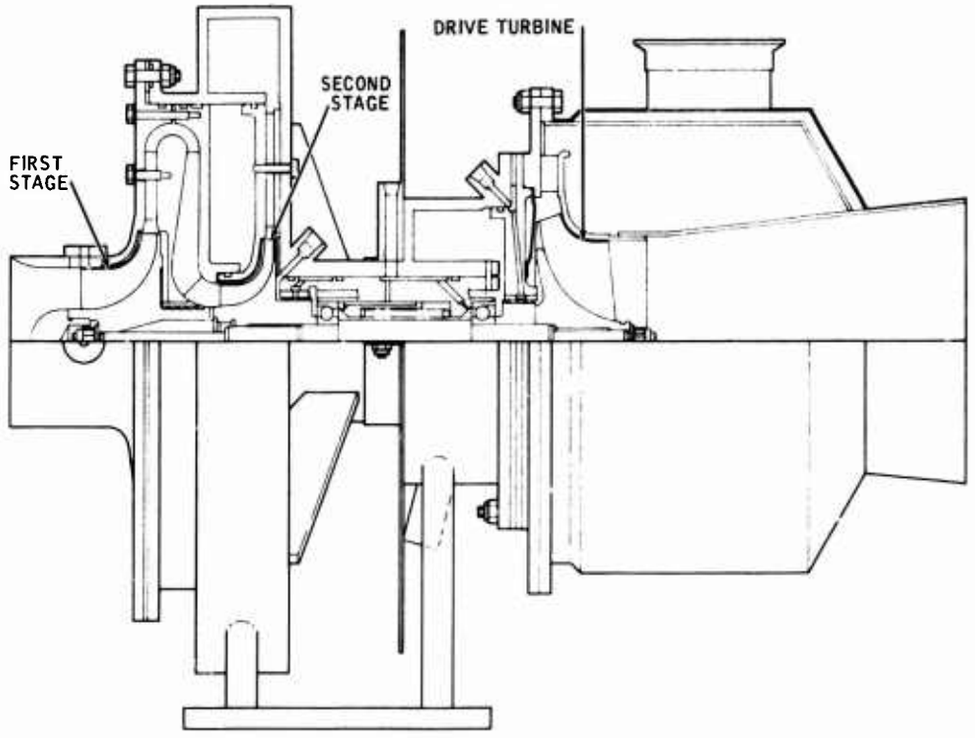

Figure 10. Compressor Rig Cross Section.

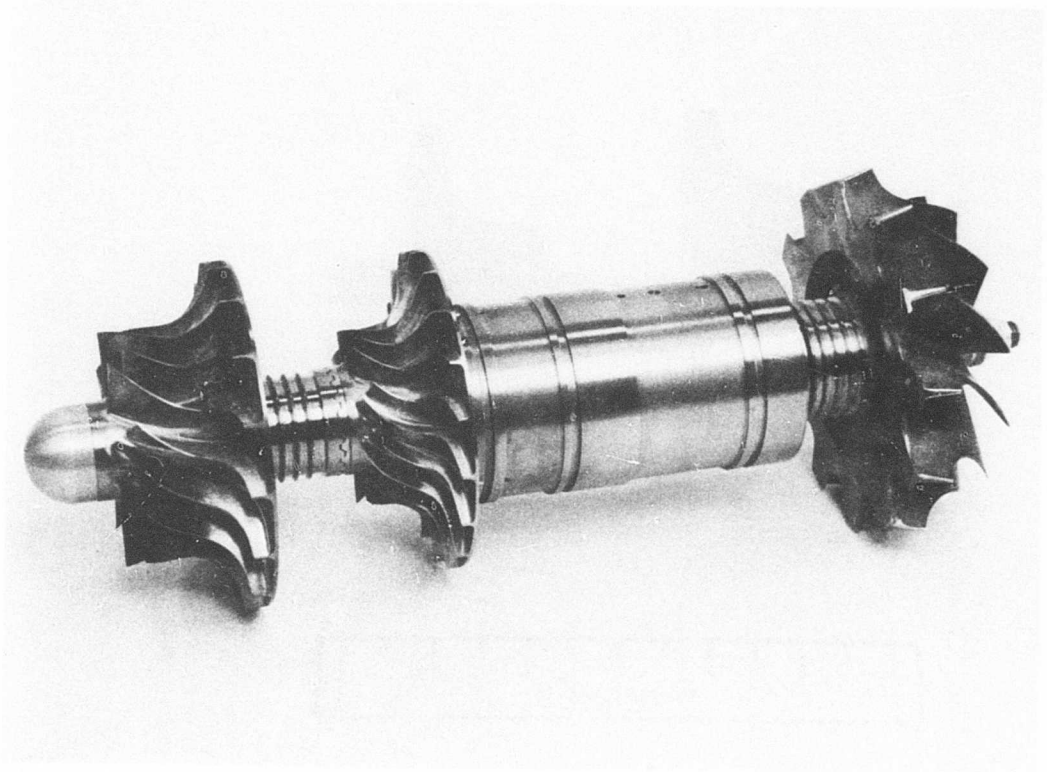

Figure 11. Rotating Assembly and Bearing Capsule.

The compressor discharge collector scroll casing forms the supporting structure of the compressor assembly, with the front stage shroud, interstage crossover assembly, and second-stage front shroud being restrained inside the discharge scroll bore.

The entire compressor rig is supported from the discharge scroll casing and bearing housing by four 3/4-inch struts to the rig bedplate. Figure 15 shows the compressor rig installed in the test cell.

Since no permanent growth of the first- and second-stage titanium compressors was predicted at design speed, the test compressor rotors were not subjected to spin pit testing. However, the drive turbine, cast from Inco 713, was spin-tested to 87,000 rpm (105 percent design speed). Appendix I contains the results of spin tests on the drive turbine.

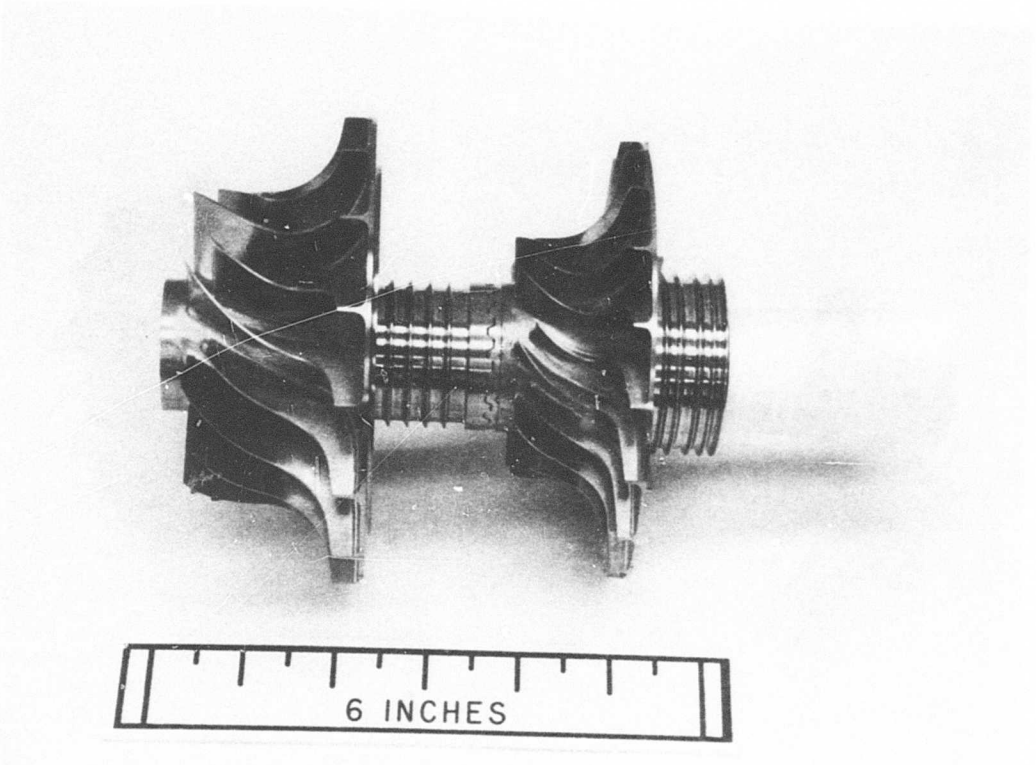

Figure 12. Impeller Assembly.

The components of the rotating assembly were all individually dynamically balanced, followed by a subsequent progressive balancing of the complete rotating group assembly.

The first- and second-stage impeller front shrouds were plasma-sprayed with an abradable aluminum epoxy material to minimize potential rubbing damage during critical speed excursions. First-stage and second-stage-impeller cold shroud clearances (radial and axial) varied from 0.013-0.019 and 0.010-0.014 respectively on the first assembly.

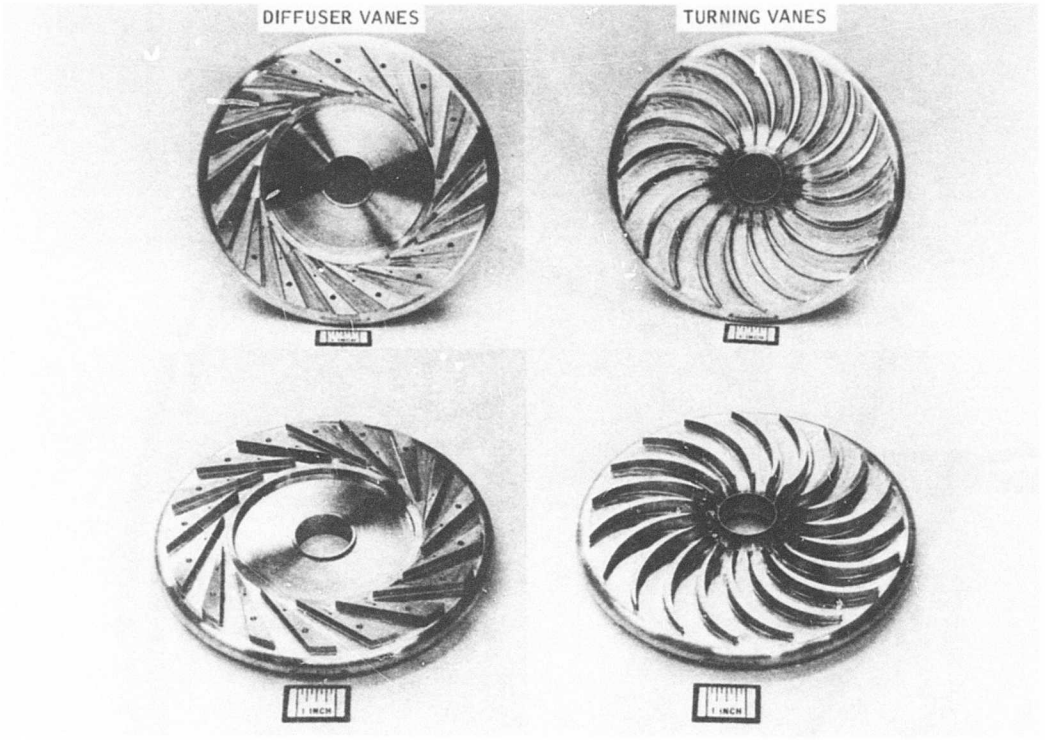

Figure 13. Interstage Crossover Assembly.

APPARATUS AND PROCEDURES

Test Cell Installation

The turbodrive package was installed in an existing test cell used specifically for testing of small advanced centrifugal compressors. Hot gas for the turbine drive was provided by plant compressed air heated to 1100°F by a natural-gas-fired in-line combustor. Automatic shutdown devices were provided to detect low oil pressure (15 psig), rotor overspeed (106 percent), high turbine inlet temperature (1500°F), and excessive bearing race temperatures (350°F). A schematic diagram of the installation is shown in Figure 16.

The compressor inlet-air system comprised a 3.0-inch-diameter ASME nozzle dumping into a 10-inch-diameter duct followed by a baffle plate situated five nozzle diameters downstream of the nozzle and eight nozzle diameters upstream of the first stage impeller. Under design speed operation the compressor inlet pressure was estimated to be 10.0 psia. An ASME 1.2-inch-diameter orifice was also used

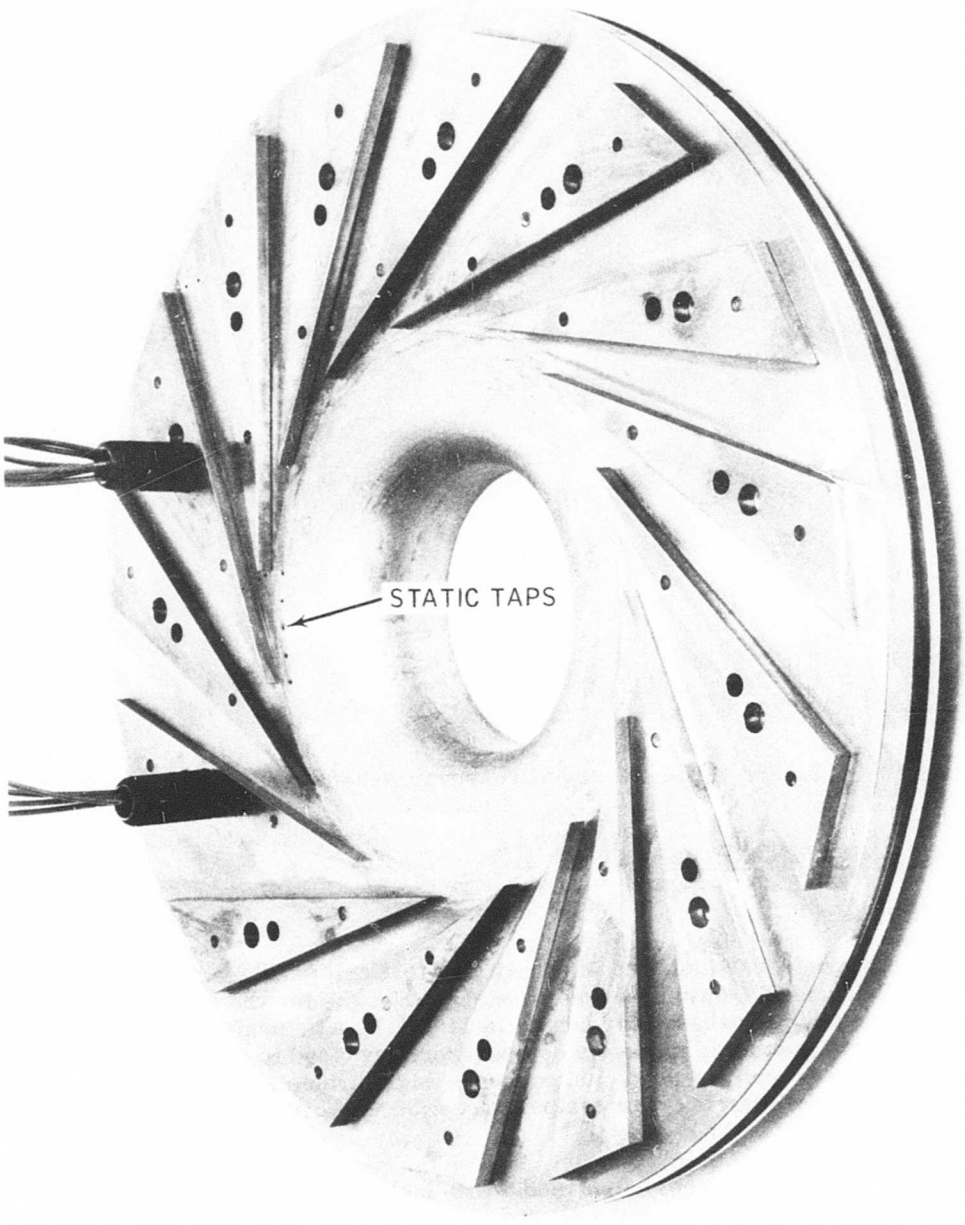

Figure 14. Second-Stage Diffuser.

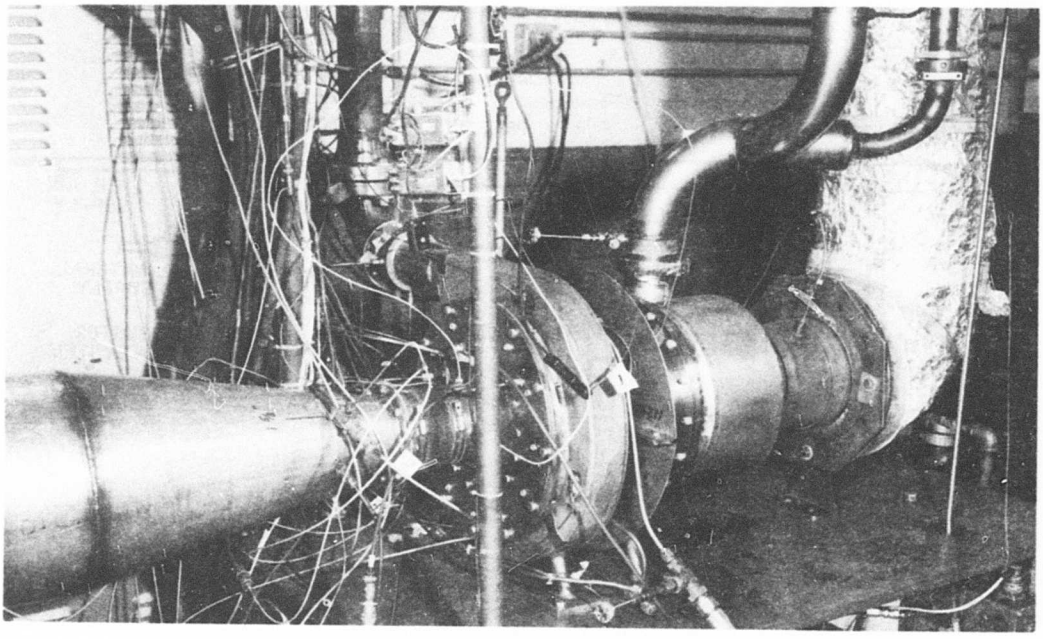

Figure 15. Installed Compressor Rig.

to measure compressor discharge flow, being placed in the discharge line downstream of the compressor discharge collector. The arrangement of the turbodrive rig and its ducting is shown in Figure 17.

Test Procedure and Operation

The turbodrive package was initially subjected to a mechanical shakedown run up to 70 percent design speed past the predicted first and second critical speeds at 27 and 42 percent design speed. The abradable first-stage shroud was inspected after the shakedown run and showed some slight evidence of abrasion along the inducer section.

The compressor performance was mapped by setting a predetermined corrected speed and gradually increasing the back pressure to determine the stable operating range. Approximately six data points evenly spaced between surge and choke were obtained for each speed line. Surge was determined audibly. Approximate time between each data point was 4 minutes.

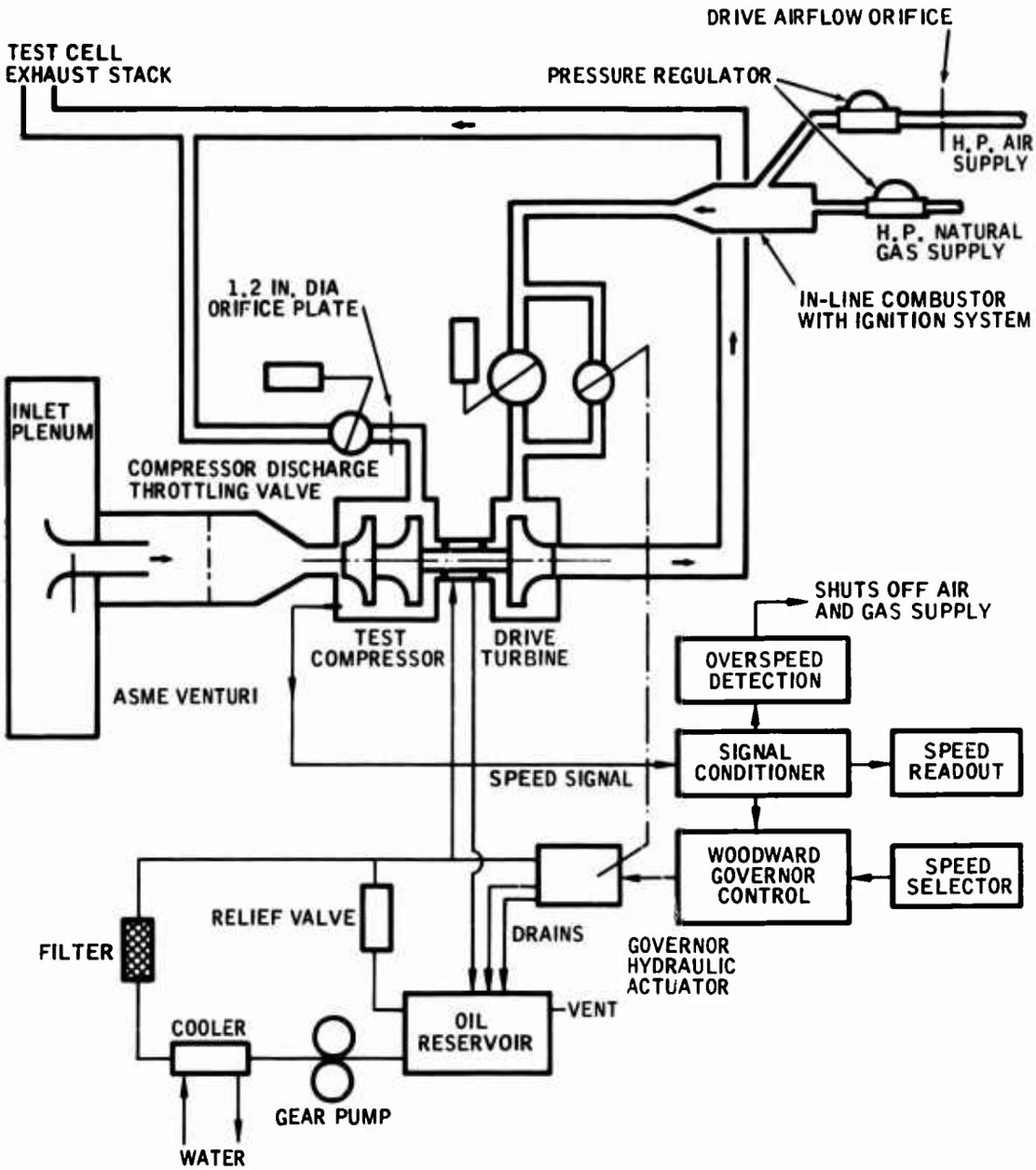

Figure 16. Test Facility Schematic.

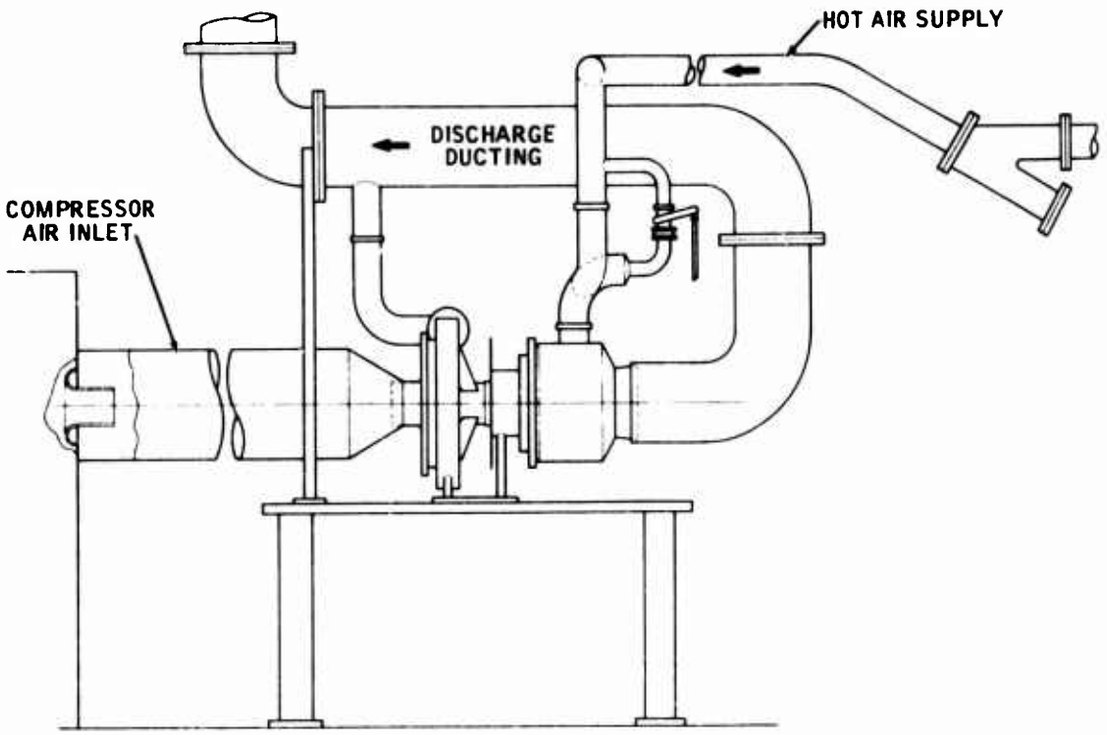

Figure 17. Compressor Test Rig Arrangement.

Due to the proximity of the second critical speed, performance mapping at 40 percent design speed was deleted and substituted by acquisition of data at an additional speed line of 70 percent design speed.

Complete data was obtained at 60, 70, 80, 90, and 95 percent design speed. Several data points were recorded at 100 percent speed, of which, only two are probably representative of valid performance potential with the proper first-stage shroud clearance. A discharge scroll casing distortion problem at 100 percent speed was experienced resulting in a progressive increase in first-stage impeller operating clearance from initial cold setting of 0.019 to final cold measurements of 0.065 to 0.070 inch.

The second-stage compressor shroud did not experience any rubbing contact. A review of the discharge scroll mechanical design and recommendations to reduce distortions at 100 percent design speed are presented in Appendix II.

Dynamic operation of the shaft system was satisfactory throughout the entire operating speed range.

Instrumentation

The instrumentation employed was divided into two categories:

1. Monitoring. Instrumentation required to monitor mechanical operation is listed in Table II.

2. Definition of compressor performance. The instrumentation listed in Table III and shown in Figure 18 was used in determining compressor performance.

Due to the small sizes of the aerodynamic passages, the number of internal probes in the compressor flow pass was limited to three, comprising two resistance thermocouples at the first-stage crossover bend and a total-pressure rake at the crossover turning vane exit. Basic reliance was upon static pressures to determine compressor performance characteristics. An error computation was conducted to determine the approximate limits of the instrumentation used to evaluate overall compressor efficiency. The results of the error computation are contained in Appendix III. Prior to installation in the test facility, the pressure transducer of the DAS system was calibrated in the instrument laboratory. Appendix IV lists the calibration results.

Calculation Procedure

The total pressure ratio, temperature rise ratio, and adiabatic efficiency were computed from the measured pressures and temperatures. Typical computer output and compressor performance parameters are listed in Appendix V. The stage and overall efficiencies presented herein were calculated using a constant specific heat ratio of 1.395. The impeller and diffuser performances were calculated from the measured static pressures at the impeller tip, diffuser throat, and diffuser exit. Flow continuity, flow area, impeller tip geometry, and temperature rise (allowing for disc friction and recirculation effects) were used to calculate average vector conditions at the impeller tip. Constant values of flow blockage were used for effective flow area determination. The impeller and diffuser performances thus calculated were used basically to assess relative component matching, without implicit acceptance of the calculated absolute efficiency and recovery levels.

Basic compressor test performance parameters compiled from the computer output are listed in Table IV for 60, 70, 80, 90, 95, and 100 percent design speed.

TEST RESULTS

Sufficient instrumentation was installed on the turbodrive two-stage centrifugal compressor rig to determine both overall-compressor and individual-stage performances.

Overall Compressor Performance

The corrected overall-compressor performance, measured with bleed take-off* prior to the first-stage vaned diffuser throat, is shown in Figure 19 for 60, 70, 80, 90, and 95 percent design speed. Also included are two

* Estimated bleed flow, based upon slot area and choking at the slot entry, with an entry pressure equal to diffuser exit total pressure was within the range of 1.5 to 2.0% first-stage inlet flow.

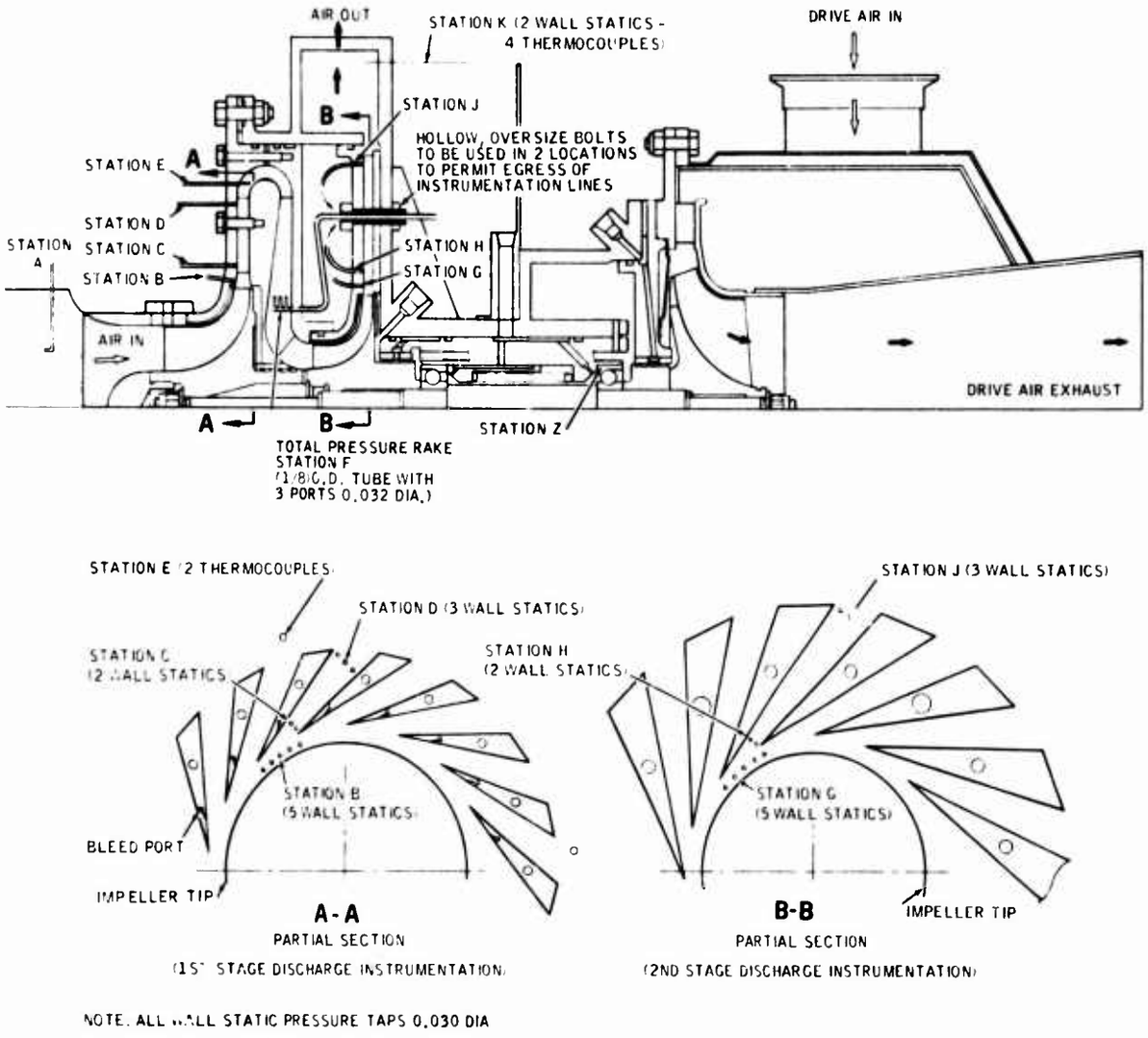

Figure 18. Two-Stage Compressor Rig Instrumentation.

performance points at 100 percent design speed taken prior to the substantial increase in first-stage impeller operating clearance, caused by distortion of the discharge scroll. The pressure ratios shown in Figure 19 are based upon compressor inlet total pressure and total pressure at the exit from the second-stage vaned diffuser with an average exit Mach number of 0.17 throughout the efficient operating range of the compressor.

The highest pressure ratio measured at 100 percent design speed (82,000 rpm corrected) was 12.3 with a corresponding overall adiabatic efficiency of 78.3 percent, and presumably some increase in first-stage impeller clearance would have already occurred at this condition. Compressor flow ranges at all speeds were very broad, providing ample surge margin for gas turbine engine matching purposes with peak efficiencies away from surge. Compressor peak overall efficiencies based upon inlet-total to discharge-scroll static pressure were approximately 1 percentage point less than total-to-total efficiencies. Note, however, that the discharge scroll was basically designed to collect the flow without any special attempts to complete further diffusion; thus, essentially no recovery of the dynamic head at the vaned diffuser discharge was required.

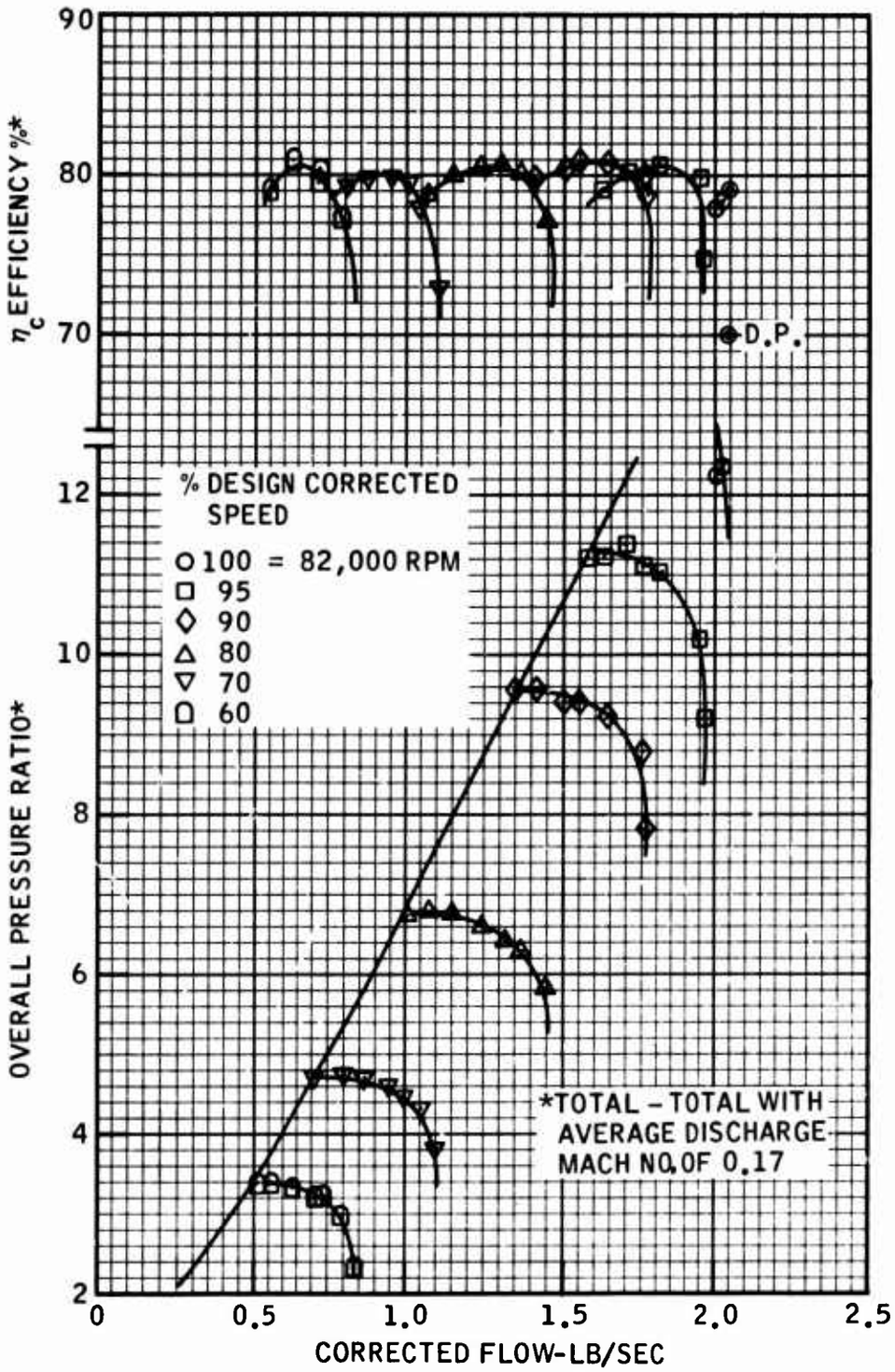

Figure 19. Overall Two-Stage Performance.

TABLE II. INSTRUMENTATION FOR MONITORING AND CONTROL OF TWO-STAGE COMPRESSOR RIG

Parameter	Sensor Type	Readout Device	Estimated Range	Remarks
Rotor Speed	——See Table III——			Automatic overspeed protection and read-out.
Rig Vibration	Accelero-meter	Charge Amplifier	0-30g	Installed adjacent to bearings. One ac-celerometer vertical and one horizontal.
Bearing Oil Supply Pressure	Wall Static	Bourdon Tube Gage	20-40 psig	Oil pressure less than 15 psig to cause automatic shutdown.
Drive Air Orifice, Upstream Pres-sure	Wall Static	Bourdon Tube Gage	0-100 psig	
Drive Air Orifice, Pressure Drop	Wall Static	Water Mano-meter		
Bearing Oil Supply Temperature	IC Full Shield Thermocouple	Self-Balancing Potentiometer	60-150 °F	
Bearing Discharge Oil Temperature	IC Full Shield Thermocouple	Self-Balancing Potentiometer	60-250 °F	
Turbine Inlet Temperature	CA Half Shield Thermocouple	Self-Balancing Potentiometer	0-1500 °F	
Turbine Exhaust Temperature	CA Half Shield Thermocouple	Self-Balancing Potentiometer	0-1100 °F	
Bearing Outer Race Temperature	IC Bare Bead Thermocouple	Self-Balancing Potentiometer	0-300 °F	One thermocouple at each bearing.
Drive Air Orifice Temperature	IC Half Shield Thermocouple	Self-Balancing Potentiometer	50-100 °F	

TABLE III. INSTRUMENTATION FOR DETERMINATION OF TWO-STAGE COMPRESSOR RIG PERFORMANCE

Parameter	Sensor Type	Recording Method	Readout Device	Estimated Range	Remarks
Rotor Speed	Proximity Probe	Manual	Digital Frequency Counter	0-11151 Hz (0-102%)	8 cycles per revolution. 100% = 82,000 rpm = 10,933 Hz.
Venturi Throat Static Pressure	Wall Static	Manual	Water Manometer	0-100 in. H_20 Depression	Average of three static taps.
	Wall Static	Automatic	Digital Voltmeter	0-4 psi Depression	Average of three static taps. (Same sensors as manual.)
First-Stage Compressor Inlet Total Pressure	Kiel Probe	Manual	Water Manometer	0-80 in. H_20 Depression	Same sensors as automatic.
	Kiel Probe	Automatic	Digital Voltmeter	0-3 psi Depression	Three probes.
First-Stage Impeller Tip Static Pressure	Wall Static	Automatic	Digital Voltmeter	0-16 psi	Five sensing ports.
First-Stage Diffuser Throat Static Pressure	Wall Static	Automatic	Digital Voltmeter	0-20 psi	Two sensing ports.
First-Stage Diffuser Vane Exit Static Pressure	Wall Static	Automatic	Digital Voltmeter	0-40 psi	Three sensing ports.
Second-Stage Inlet Total Pressure	Total Pressure Rake	Automatic	Digital Voltmeter	0-50 psi	Total pressure rake.
Second-Stage Impeller Tip Static Pressure	Wall Static	Automatic	Digital Voltmeter	0-90 psi	Five sensing ports.

TABLE III - Continued

Parameter	Sensor Type	Recording Method	Readout Device	Estimated Range	Remarks
Second-Stage Diffuser Throat Static Pressure	Wall Static	Automatic	Digital Voltmeter	0-100 psi	Two sensing ports.
Second-Stage Diffuser Vane Exit Static Pressure	Wall Static	Automatic	Digital Voltmeter	0-140 psi	Three sensing ports.
Second-Stage Discharge Static Pressure	Wall Static	Manual	Hiese Gage	0-150 psi	Same sensors as automatic.
	Wall Static	Automatic	Digital Voltmeter	0-150 psi	Two sensing ports.
Air Inlet Plenum Temperature	RTD*	Automatic	Digital Voltmeter	50-90°F	One RTD
First-Stage Compressor Inlet Temperature	RTD	Automatic	Digital Voltmeter	50-90°F	Three RTD
First-Stage Compressor Delivery Temperature	RTD	Automatic	Digital Voltmeter	0-300°F	Two RTD
Second-Stage Compressor Delivery Temperature	RTD	Automatic	Digital Voltmeter	0-850°F	Four RTD
Turbine Inlet Static Pressure	Wall Static	Manual	Bourdon Tube Gage	0-80 psi	Same sensor as automatic.
		Automatic	Digital Voltmeter	0-80 psi	One sensing port.

* Resistance Temperature Detectors

TABLE IV. COMPRESSOR TEST PERFORMANCE PARAMETERS

		OVERALL				FIRST STAGE					SECOND STAGE						
DP	BLEED %	$N/\sqrt{\theta_1}$ x 10^{-3}	$W\sqrt{\theta_1}/\delta_1$	P_2/P_1	η_c	P_2/P_1	$\eta_{1\text{-}E}$	$\eta_{1\text{-}2}$	CP 2-E	q	$N/\sqrt{\theta_1}$ x 10^{-3}	$W\sqrt{\theta_1}/\delta_1$	P_2/P_1	$\eta_{1\text{-}E}$	$\eta_{1\text{-}2}$	CP 2-E	q
1	1.5	49.1	.829	2.29	.570	1.951	.865	.894	.825	.650	44.1	.473	1.172	.257	.919	.790	.678
2		49.2	.780	3.05	.774	1.975	.851	.879	.842	.671	44.0	.441	1.547	.712	.936	.280	.699
3		49.1	.721	3.22	.805	1.980	.840	.871	.842	.687	43.8	.408	1.630	.794	.949	.480	.716
4		49.1	.627	3.36	.807	1.998	.821	.857	.846	.712	43.7	.353	1.680	.821	.949	.578	.743
5		49.1	.537	3.41	.787	1.992	.784	.840	.799	.742	43.5	.304	1.713	.828	.949	.617	.774
6		49.1	.501	3.41	.785	SURGE						.284	1.711				
7		49.2	.709	3.20	.792	1.977	.831	.867	.829	.690	43.9	.402	1.619	.777	.935	.472	.719
8		57.3	1.090	3.84	.726	2.401	.848	.907	.737	.658	49.7	.524	1.597	.617	.925	.048	.686
9		57.2	1.036	4.27	.778	2.420	.838	.889	.768	.674	49.5	.495	1.763	.745	.930	.386	.703
10		57.1	.989	4.43	.794	2.432	.834	.881	.787	.684	49.3	.471	1.822	.785	.938	.484	.713
11		57.2	.930	4.58	.796	2.447	.821	.868	.799	.699	49.2	.442	1.870	.808	.937	.562	.729
12		57.2	.866	4.68	.795	2.452	.807	.856	.800	.713	49.1	.412	1.907	.824	.934	.625	.743
13		57.2	.697	4.71	.787	SURGE						.332	1.901				
14		57.2	.795	4.73	.790	2.452	.794	.846	.797	.724	49.0	.379	1.931	.831	.932	.661	.755
15		65.4	1.434	5.83	.771	2.999	.835	.911	.683	.665	54.6	.573	1.943	.738	.932	.354	.693
16		65.4	1.360	6.31	.801	3.056	.837	.902	.726	.675	54.4	.535	2.065	.802	.933	.538	.704
17		65.3	1.308	6.41	.807	3.073	.839	.897	.752	.682	54.3	.512	2.087	.813	.937	.566	.711
18		65.4	1.232	6.58	.802	3.081	.822	.877	.767	.695	54.2	.483	2.135	.828	.935	.622	.724
19		65.4	1.126	6.72	.796	3.100	.808	.861	.786	.712	53.9	.440	2.169	.834	.932	.658	.743
20		65.3	.979	6.71	.785	SURGE						.385	2.176				
21		65.3	1.063	6.74	.787	3.089	.795	.851	.780	.722	53.8	.418	2.181	.834	.931	.670	.728
23		73.3	1.534	9.39	.807	3.826	.810	.870	.751	.691	58.4	.503	2.454	.863	.942	.709	.720
24		73.2	1.409	9.54	.797	3.856	.798	.857	.760	.709	58.2	.460	2.474	.859	.935	.727	.739
25		73.2	1.332	9.52	.782	SURGE						.435	2.461				
26		73.2	1.500	9.38	.803	3.822	.805	.866	.750	.697	58.3	.492	2.456	.861	.941	.707	.726
27		73.4	1.627	9.26	.806	3.803	.812	.880	.720	.684	58.6	.535	2.436	.859	.941	.691	.713
28		73.4	1.755	8.75	.799	3.714	.815	.889	.689	.667	58.9	.589	2.356	.836	.939	.618	.695
38		73.7	1.739	7.85	.745	3.556	.786	.878	.627	.657	59.2	.609	2.207	.759	.918	.450	.693

TABLE IV - Continued

		OVERALL				FIRST STAGE					SECOND STAGE						
DP	BLEED %	$N/\sqrt{\theta_1}$ x 10^{-3}	$\frac{W\sqrt{\theta_1}}{\delta_1}$	$\frac{P_2}{P_1}$	η_c	$\frac{P_2}{P_1}$	η_{1-E}	η_{1-2}	CP 2-E	q	$N/\sqrt{\theta_1}$ x 10^{-3}	$\frac{W\sqrt{\theta_1}}{\delta_1}$	$\frac{P_2}{P_1}$	η_{1-E}	η_{1-2}	CP 2-E	q
31	1.5	77.3	1.935	10.15	.796	4.062	.819	.881	.718	.648	61.2	.602	2.500	.827	.932	.614	.702
32		77.7	1.806	11.02	.806	4.247	.819	.878	.745	.667	61.0	.541	2.593	.853	.935	.695	.716
33		77.8	1.737	11.08	.794	4.251	.798	.862	.733	.683	60.8	.522	2.606	.857	.937	.710	.722
34		77.5	1.624	11.22	.790	4.278	.791	.855	.737	.697	60.5	.487	2.623	.861	.935	.730	.733
35		77.5	1.574	11.17	.789	SURGE						.473	2.621				
36		77.7	1.709	11.42	.802	4.390	.815	.866	.780	.687	60.7	.498	2.601	.850	.924	.727	.728
39		77.8	1.955	9.17	.745	3.903	.775	.876	.590	.652	61.3	.635	2.348	.779	.921	.493	.684
44		81.9	2.029	12.32	.783	4.563	.787	.856	.701	.663	63.1	.577	2.701	.853	.933	.694	.702
45		81.9	1.983	12.31	.776	4.623	.783	.856	.695	.673	62.9	.558	2.664	.844	.932	.675	.703
46											63.5	.638	2.550	.805	.913	.600	.690
47											62.8	.554	2.622	.833	.913	.697	.700
48											63.3	.576	2.607	.842	.913	.711	.680

Estimated design-point overall compressor performance was a peak efficiency of 79 percent at a pressure ratio of 14.0 with a corrected airflow of 2.05 pps, compared to the highest pressure ratio measured at 100 percent design speed on test of 12.3, with a corresponding efficiency and airflow of 78.3 percent and 2.03 pps respectively.

The basic reasons for lower performance than design were:

1. The progressive increase in first-stage axial clearance caused by distortion of the discharge scroll at 100 percent design speed, decreasing the efficiency of the first-stage compressor.

2. Lower-than-design pressure-ratio capability of the second stage.

The separate performances of the two stages are discussed below.

First-Stage Performance

Overall performance of the first-stage compressor, with approximately 1.5 percent bleed flow at the vaned diffuser slots, is shown in Figure 20 for 60, 70, 80, 90, and 95 percent design speed. Also included are two performance points at 100 percent design speed acquired prior to the substantial increase in first-stage impeller operating clearance caused by distortion of the discharge scroll. The pressure ratios shown in Figure 20 refer to total pressure at the stage inlet and total pressure at the exit of the interstage crossover turning vanes, with an average exit Mach number of 0.17 throughout the efficient operating range of the compressor.

Estimated design-point first-stage compressor performance was a peak efficiency of 81 percent at a pressure ratio of 4.9 with a corrected airflow of 2.05 pps, compared to test performance of 100 percent speed (data point 44, presumably with some increased shroud clearance) of 78.7 percent with a pressure ratio of 4.56 and corrected airflow of 2.03 pps. After completion of running at 100 percent speed with the shroud clearance increased to 0.065 to 0.070 inch, the efficieny of the first-stage compressor had decreased to the 70 percent level. Peak first-stage efficiency at 90 and 95 percent design speed was 81.5 percent, increasing to 86 percent at 60 percent design speed.

Relative matching of the first-stage impeller and its vaned diffuser is shown in Figure 21. The highest test-impeller efficiency calculated at 100 percent speed was 85.5 percent with a corresponding overall diffusion system (including interstage crossover) static pressure recovery CP_{2-E} of 0.70 and work factor q of 0.67. The high speed matching confirms that the impeller is approaching its peak efficiency in the regions of maximum diffusion system static pressure recovery, particularly at 95 percent design speed. More data is required at 100 percent design speed to confirm optimized matching. Note that even if the first stage had attained its design overall efficiency of 81 percent at design airflow, its pressure ratio (at that single test condition) would probably have been slightly reduced at 4.76, since the test work factor was 0.67 compared to 0.68 design. The true performance potential of the first stage cannot adequately be determined

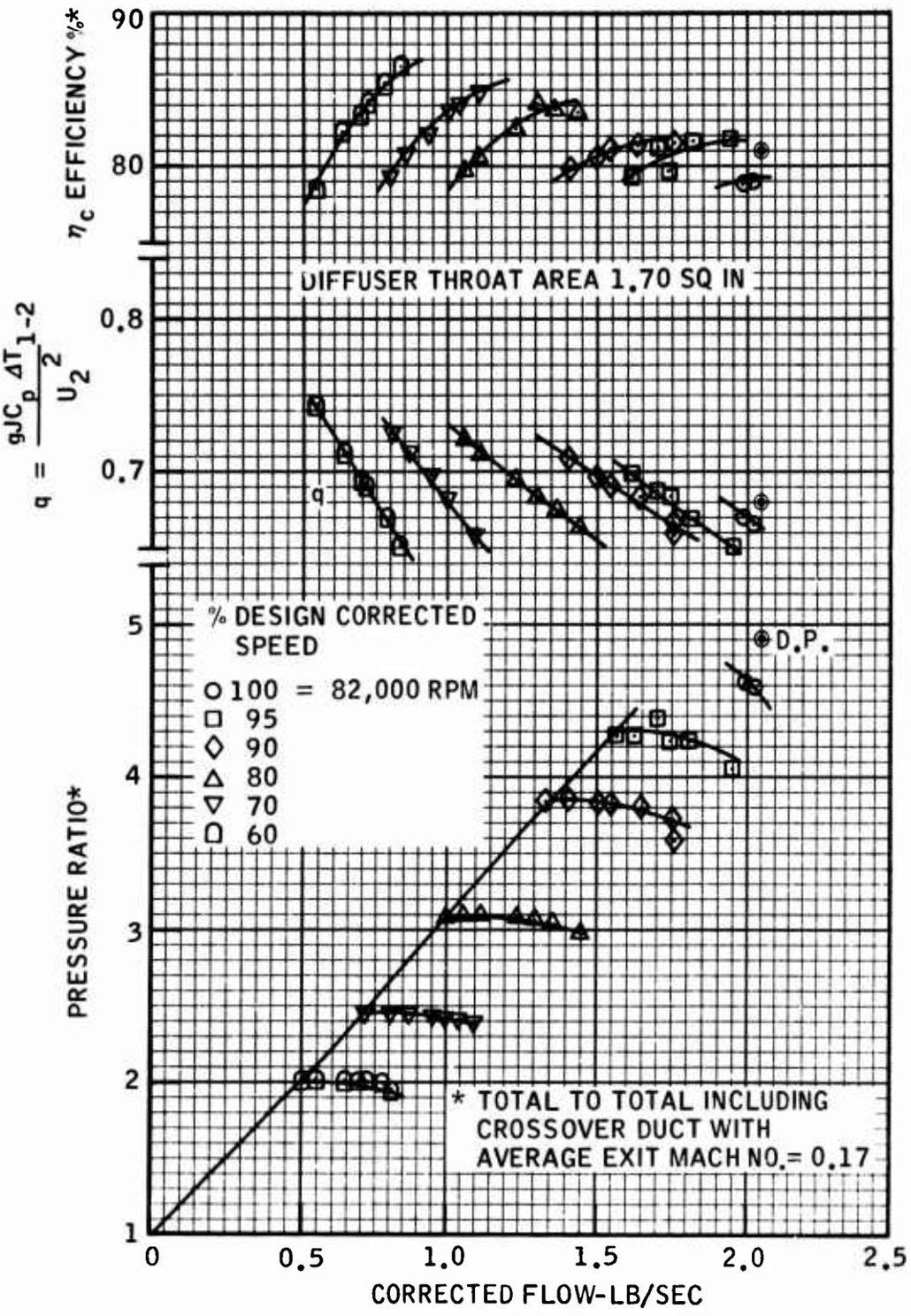

Figure 20. First-Stage Characteristic.

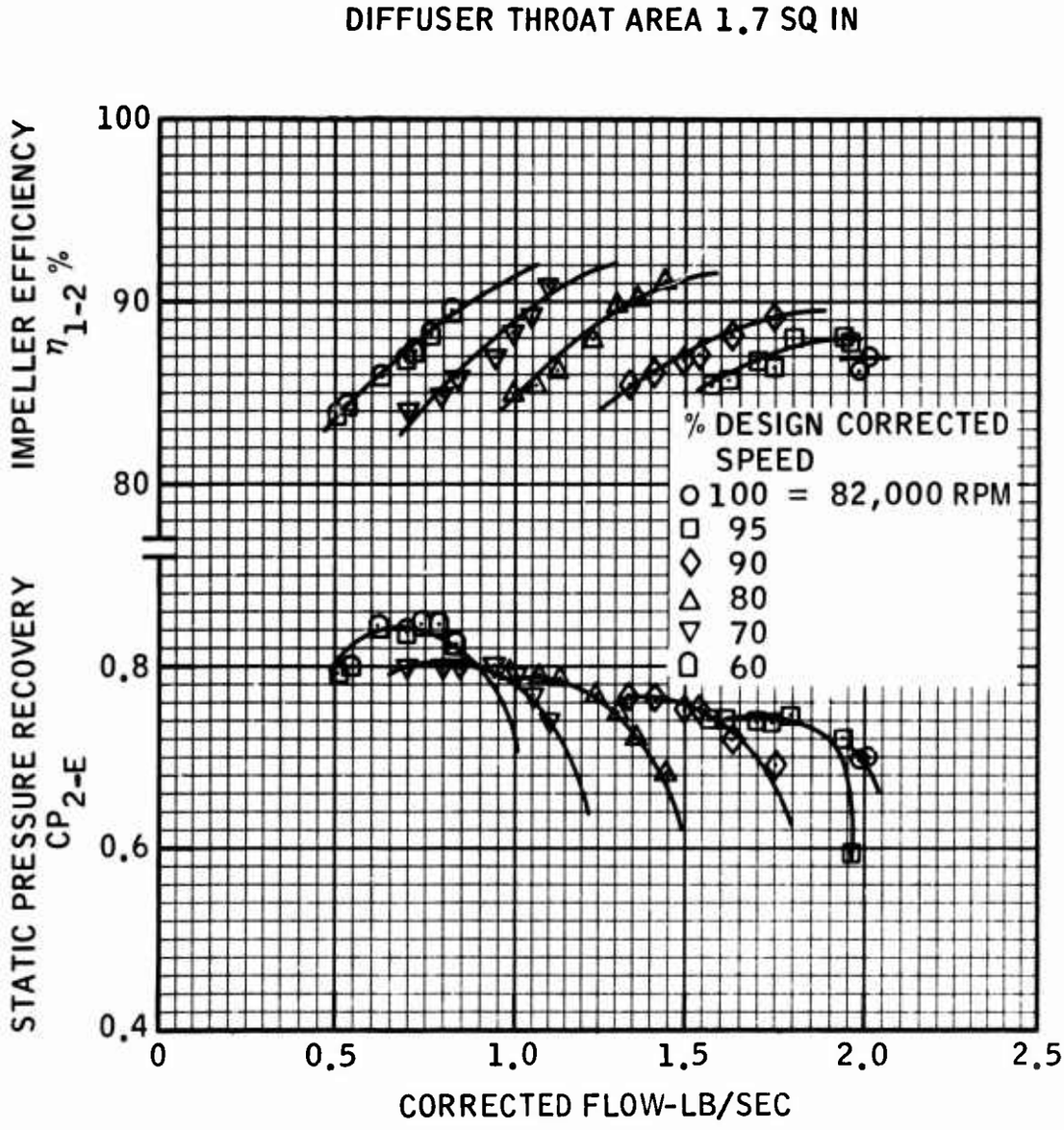

Figure 21. First-Stage Impeller and Diffuser Matching.

at this point due to insufficient data. However, it does appear from the adjacent speed data that with the correct clearance it should be possible to approach design efficiency and airflow. Figure 22 shows the pressure loss of the interstage crossover between exit of the first-stage vaned diffuser and exit of the interstage turning vanes. Equivalent loss in stage efficiency is of the order of 2 percentage points in the peak efficiency operating range. It is doubtful if this loss can be significantly reduced by redesign, and it must be accepted as an inherent penalty associated with staging two compressors in series.

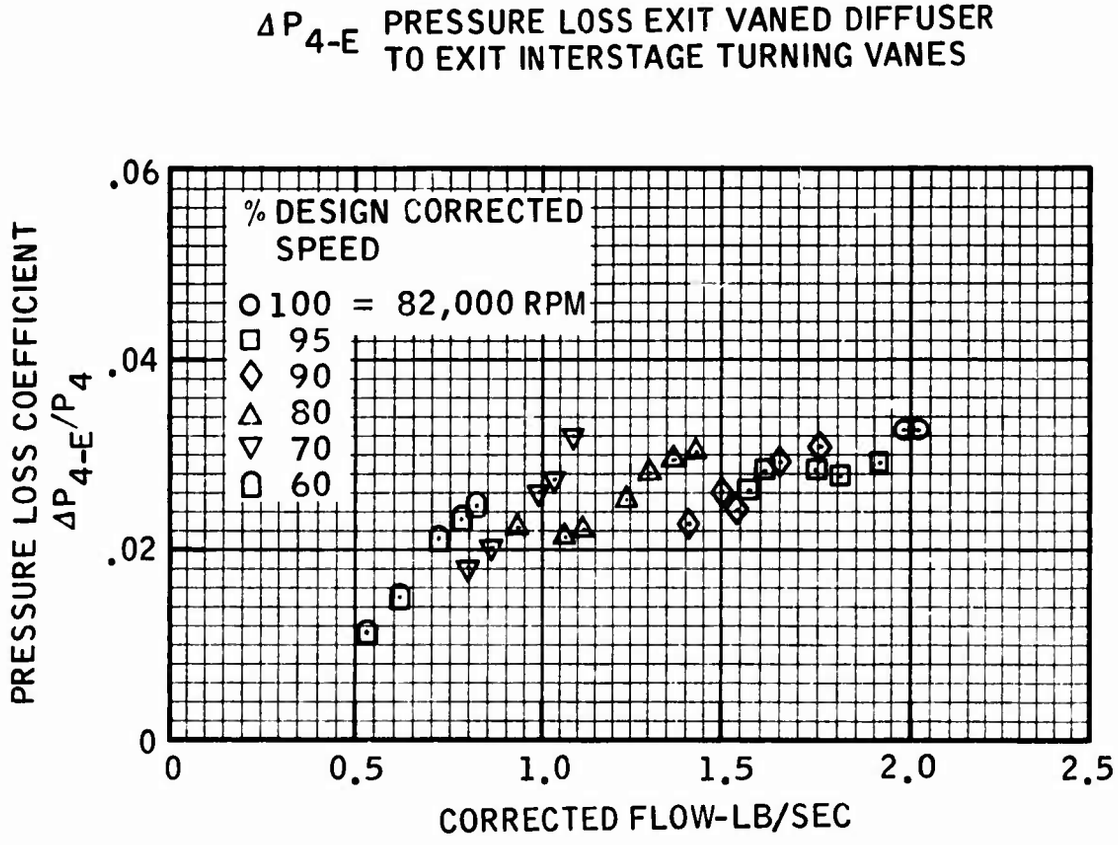

Figure 22. Interstage Crossover Pressure Losses.

Second-Stage Performance

Overall performance of the second-stage compressor is shown in Figure 23 at the various average* test-corrected speeds based upon second-stage inlet temperature. The pressure ratios shown in Figure 23 refer to total pressure at the stage inlet and total pressure at the vaned diffuser exit, with an average discharge Mach number of 0.17 throughout the efficient operating range of the second stage.

Valid 100 percent performance data was obtained for the second stage at several airflows. At the second-stage design speed and corrected airflow, the test pressure ratio, adiabatic efficiency, and work factor were 2.70, 84 percent, and 0.705 respectively; this compares to respective design values of 2.86, 83 percent, and 0.758. The major reason for decreased pressure ratio is the lower compressor test work factor q of 0.705, possibly due to higher entry prewhirl to the second stage. The interstage crossover turning vanes were designed to accomplish 63 degrees of air turning with a residual exit prewhirl of 7.0 degrees in the direction of rotation. A residual prewhirl of the order 20 degrees might explain the lower test work factor, but could only be confirmed by extensive traversing in the relatively inaccessible region of the second-stage inducer entry. Note that the test Reynolds number for the second stage was some 30 percent higher than the baseline single stage tests with ambient suction conditions. Methods of increasing the pressure ratio to the design level would be an increase in either rotational speed or impeller tip diameter of approximately 3 percent.

Relative matching of the second-stage impeller and its vaned diffuser is shown in Figure 24. Peak impeller efficiency and diffuser static pressure recovery (calculated assuming an inlet prewhirl of 7.0 degrees) are shown versus inlet corrected flow at the various test speeds. Peak impeller efficiency and diffuser static pressure recovery at design speed and flow were 92.5 percent and 0.71 respectively, compared to design values of 91 percent and 0.73.

Compressor Surge

The compressor surge line was determined by gradually closing the discharge throttle until audible surge (compressor stall) was observed at the test speeds. Figure 25 compares the estimated and test performance data, with 1.5 percent first-stage diffuser

---

* Due to the inherent characteristics of backswept compressors, maintaining a constant first-stage corrected speed does not truly provide constant corrected-speed conditions at the second-stage inlet.

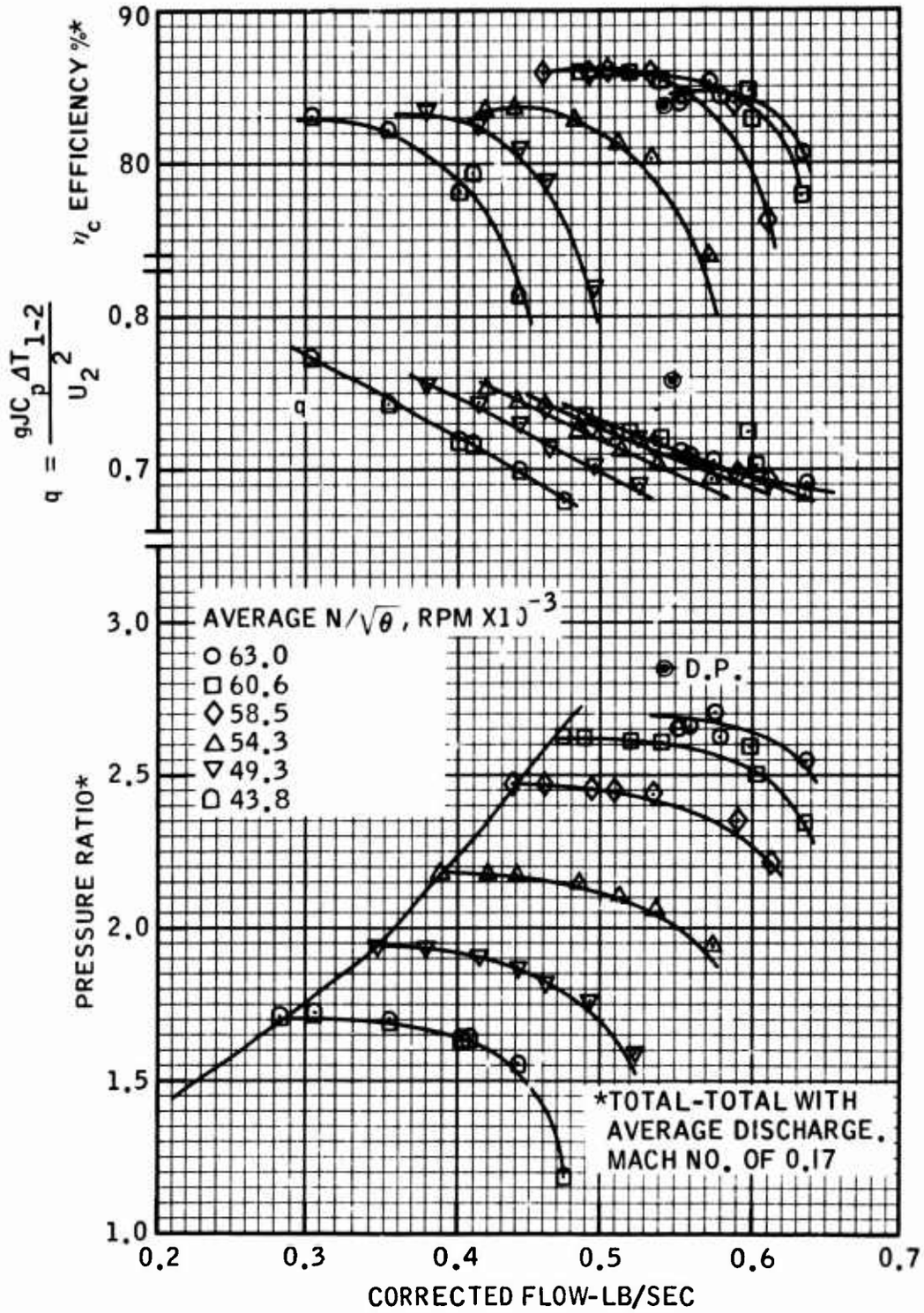

Figure 23. Second-Stage Characteristic.

bleed, to the surge lines predicted for the first and second stages from individual stage tests on the two baseline compressors from which the two-stage unit was scaled. It had been conservatively anticipated that the overall compressor surge line would follow that of the baseline first stage, whereas overall surge was in fact practically coincident with the baseline second-stage surge line. Comparisons of the baseline first-stage surge line (zero bleed) with the surge flows exhibited during test indicated that the first stage was operating well beyond its baseline surge limit. Without completing tests with and without diffuser slot bleed, it cannot be conclusively stated that the slot bleed is the major reason for the large flow range exhibited on test. It is even possible that the second stage could have been stabilizing the first stage to operate beyond stall. Nevertheless, the effect of slot bleed on similar Solar single-stage compressors has shown significant improvements in surge line characteristics. It is recommended that, during continuation tests, the effect of diffuser slot bleed on both surge line and overall compressor performance be thoroughly investigated.

Examination of the overall compressor performance (Figure 19), with respect to possible application in a small turboshaft gas turbine with fixed turbine geometry, substantiates design predictions that operation at high pressure ratios can be achieved on a two-stage centrifugal compressor without the necessity for variable stator regulation. The flow ranges are very broad; this, together with a linear surge line and a large island of 79 percent efficiency, represents a considerable technology improvement in small high-pressure-ratio compressors.

PERFORMANCE SUMMARY

Analysis of the overall and stage test performances of the subject two-stage centrifugal compressor leads to revised predictions of performance level. These are listed in Table V.

With the current component matching, and the discharge scroll modified to ensure the proper first-stage operating clearances, it is estimated that it should be possible to attain a pressure ratio of 12.7 with an efficiency of 78.7 percent at design speed and airflow. In order to attain design pressure ratio with the current matching and modified scroll, it will be necessary to increase the rotational speed by 3 percent; under these conditions, the estimated overall efficiency would be 78.2 percent. An alternate, more costly option to increasing the speed would be to increase the impeller tip diameters by 3 percent. It should be emphasized that these predictions are based upon the measured test performance at 100 percent speed when some slight first-stage performance deterioration could have already occurred. Additionally, in many gas turbine applications, some high speed (100 percent) degradation of compressor performance is permissible if higher efficiencies are exhibited at operating conditions equivalent to 60 percent and 30 percent maximum rated engine output. In this instance, peak test efficiencies at all speeds up to 95 percent design speed were 2 percentage points higher than design-point efficiency.

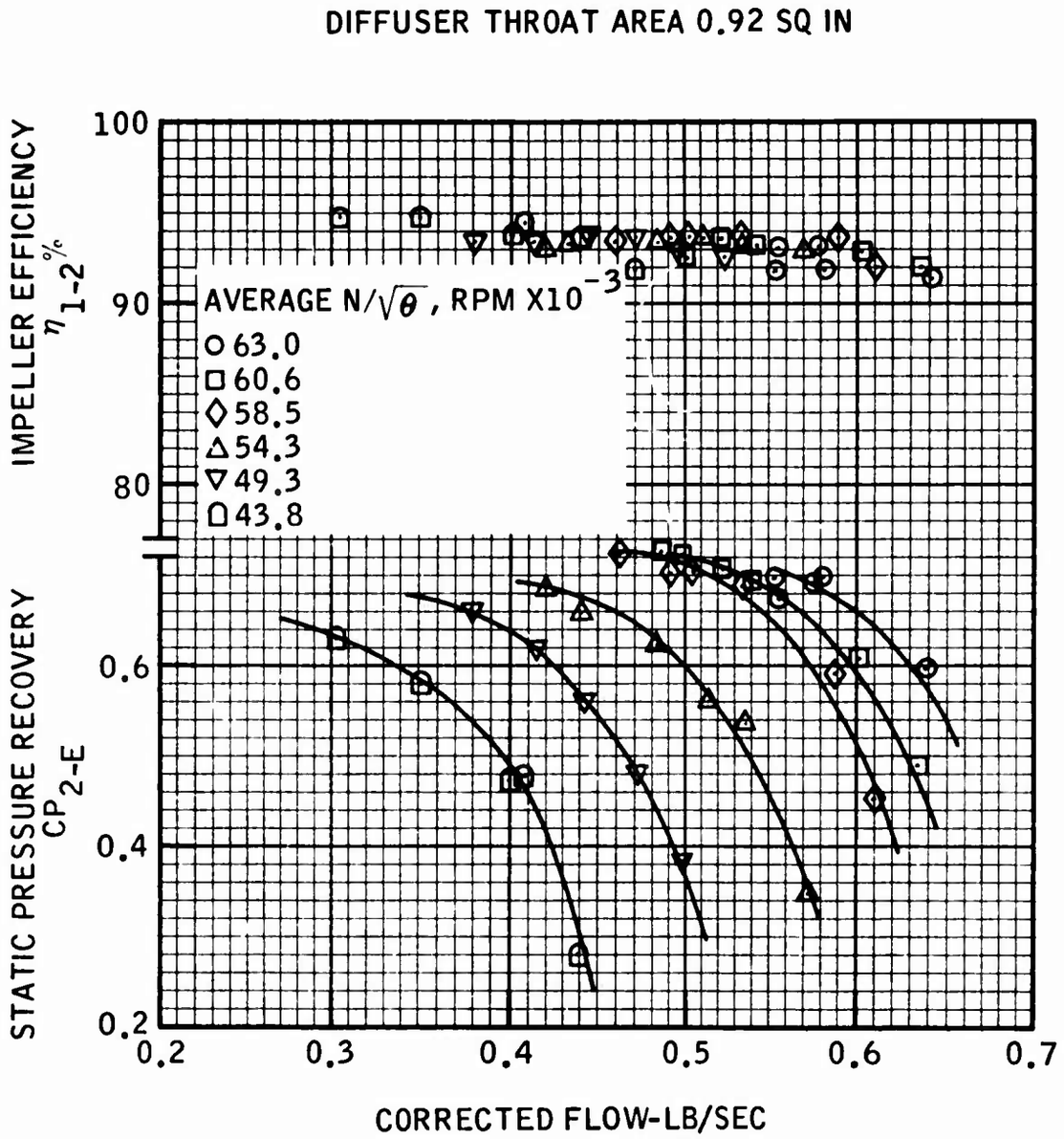

Figure 24. Second-Stage Impeller and Diffuser Matching.

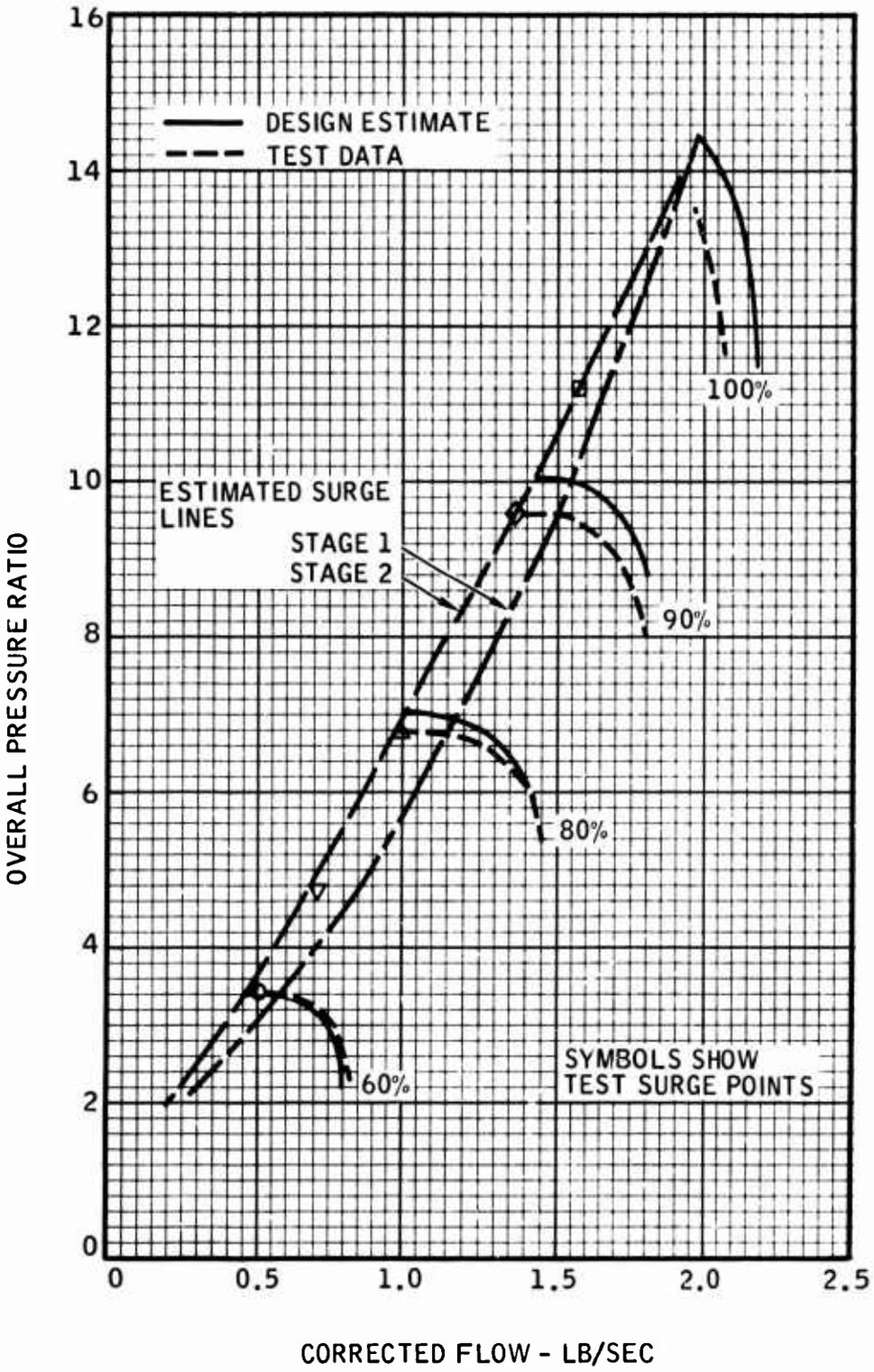

Figure 25. Compressor Map Comparison.

TABLE V. COMPRESSOR PERFORMANCE COMPARISONS

Item	Case*			
	1	2	3	4
Rotational Speed, rpm x 10^{-3}	82	82	82	84.5
Inlet Pressure, psia	14.7	14.7	14.7	14.7
Inlet Temperature, °F	60	60	60	60
Inlet Airflow, pps	2.05	2.03	2.05	2.1
First-Stage Pressure Ratio	4.9	4.56	4.7	4.95
**First-Stage Efficiency, %	81.0	78.7	80.0	79.5
Second-Stage Pressure Ratio	2.86	2.70	2.70	2.83
**Second-Stage Efficiency, %	83.6	85.3	84.0	84.0
Overall Pressure Ratio	14.0	12.3	12.7	14.0
**Overall Efficiency, %	79.0	78.3	78.7	78.2

*Case:

1. Original design.
2. Test data point 44. (See Appendix V.)
3. Estimated, with current matching and modified discharge scroll.
4. Same as case 3 except speed increased by 3%.

** All efficiencies based on discharge total condition with an average Mach number of 0.17.

CONCLUSIONS

Complete performance test data was obtained for the subject two-stage centrifugal compressor at 60, 70, 80, 90, and 95 percent speed showing peak overall temperature rise adiabatic efficiencies up to 80.5 percent at pressure ratios between 3.4 and 11.2.

A compressor discharge scroll casing distortion problem at 100 percent design speed (82,000 rpm) prevented accurate assessment of design speed performance capability. Although several data points were recorded at 100 percent design speed, only two were probably representative of valid performance potential. The highest pressure ratio was 12.3 with a corresponding overall adiabatic efficiency of 78.3 percent.

The compressor exhibited broad compressor flow ranges between the surge and choke flows, substantiating design predictions that operation at high pressure ratio could be obtained on a two-stage centrifugal compressor without the necessity for variable stator regulation.

The mechanical design of the rotating assembly, with the two stages overhung from a central bearing capsule, proved successful.

It is predicted that, with modifications to prevent distortion of the discharge scroll casing, it should be possible to obtain design performance at 3 percent overspeed condition with the current component matching.

RECOMMENDATIONS

First run testing of the subject two-stage centrifugal compressor has revealed performance characteristics which represent a considerable technology improvement in small high-pressure-ratio compressors for advanced gas turbines. As a consequence of these encouraging first test results, the following additional tasks are recommended to increase and more closely define the compressor performance potential:

1. Modify the compressor discharge scroll to prevent first stage shroud distortion problems.

2. Conduct performance calibrations and 100 percent design speed with 1.5 percent first-stage diffuser bleed.

3. Repeat performance testing with diffuser bleed closed.

4. Conduct overspeed testing to 103 percent design speed equal to a corrected speed of 84,500 rpm.

5. Pursuant with analysis of the previous testing, conduct an additional test with a diffuser rematch to optimize performance.

APPENDIX I
DRIVE TURBINE SPIN TEST RESULTS

Due to the very high rotational speeds to be encountered while operating the USA AMRDL two-stage compressor test rig, it was required to ensure the mechanical integrity of the rig turbine wheel and stress relieve the bore by proof spinning. A bore radial growth of 0.004 inch was predicted at 100% design speed.

The turbine wheel was a Solar Titan 713LC production casting that had a modified hub and shortened blade tips. Prior to proof spinning, the wheel was balanced to within 0.003 ounce-inches of residual unbalance. The piloting bore diameters and the blade tip diameter were measured and recorded.

On April 5, 1972, the turbine wheel was successfully proof spun in the Solar spin pit for 1 minute at an approximate speed of 87,000 rpm (106 percent of rig design speed of 82,000 rpm). A special spin arbor was used to spin the wheel. After proof spin, the bore and blade tip diameters were remeasured and recorded. Up to 0.0072 inch of bore diameter growth and up to 0.0073 inch of blade tip diameter growth resulted from the proof spin. Both visual and Zyglo inspection of the wheel revealed no defects.

The turbine wheel was deemed to be mechanically sound for use in the compressor test rig. The wheel was then reworked to design dimensions and installed in the rig.

APPENDIX II
COMPRESSOR SCROLL STRESS ANALYSIS FOR TWO-STAGE COMPRESSOR TEST RIG

Stresses and deflections were computed for the subject scroll to establish a computation model giving results consistent with the observed permanent distortions that occurred in the test rig; specifically, in the -25, -26, and -27 parts. Figure 26 shows the assumed model shell element centerline geometry with the linear temperature gradient and pressure load.

Stress and deflection calculations were made using two different analytical techniques: a two-dimensional finite element program and a shell analysis program. Both methods gave deflections consistent with the measured pattern of distortion observed in the test rig, and indicated stresses greater than the material yield strength (24 ksi at 500°F and 22 ksi at 800°F), confirming the permanent distortion.

The effect of the degree of restraint imposed at edge A (Figure 26) was evaluated by running two cases:

(1) Full radial restraint.

(2) No radial restraint.

The true case would lie between these limits. Case (1) gave higher stresses, but both cases indicated material yielding.

It would appear that scroll design changes can be properly evaluated to give controlled deflection and stress characteristics under load.

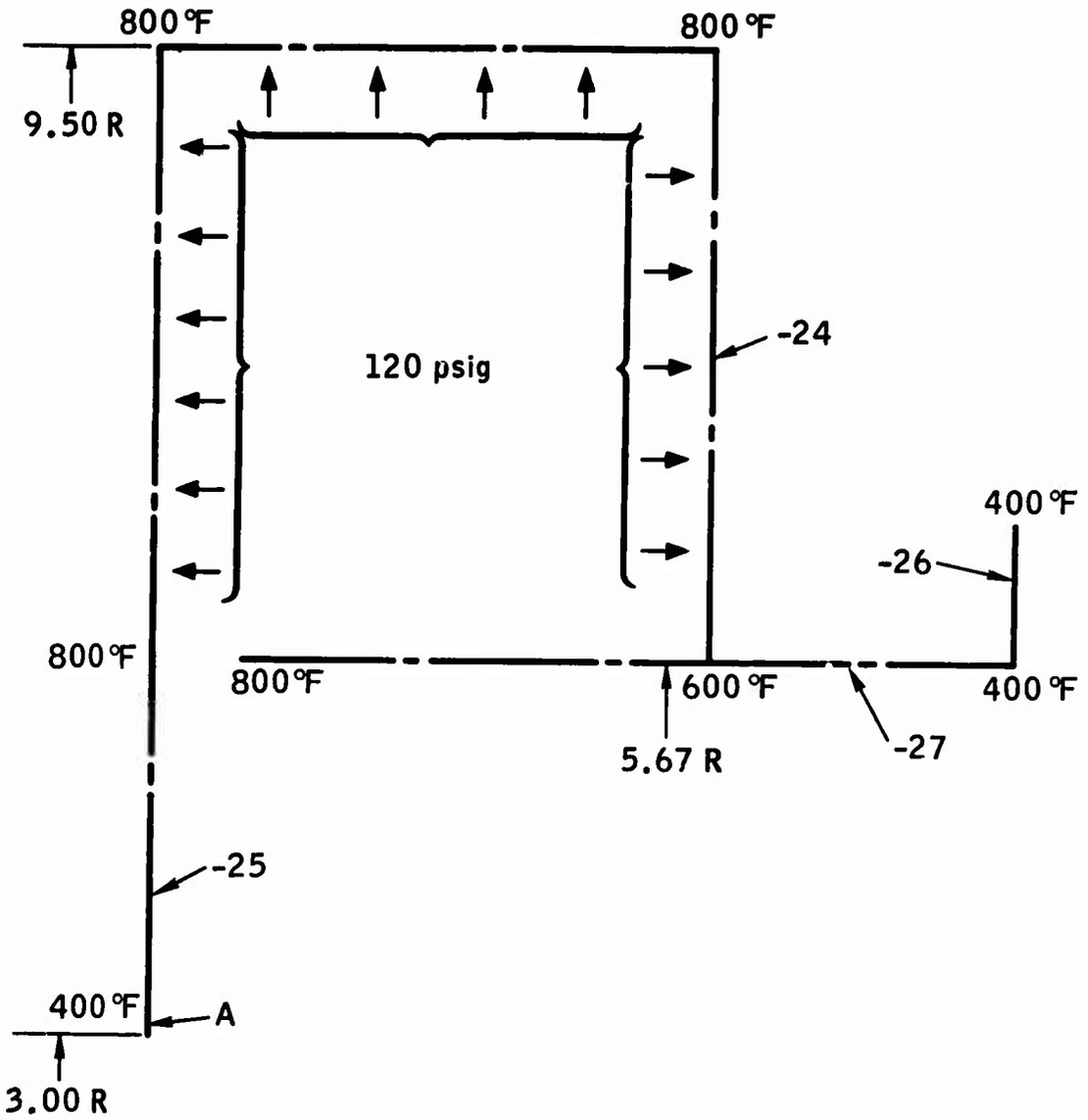

Figure 26. Two-Stage Compressor Test Rig Scroll Centerline Geometry for Stress Calculation.

APPENDIX III
ERROR COMPUTATION FOR TWO-STAGE COMPRESSOR

Design Conditions:

$$\eta_c = \frac{\left(\frac{P_E}{P_1}\right)^{\frac{\gamma-1}{\gamma}} - 1}{\frac{\Delta T_{1-E}}{T_1}}$$

At design point:

P_1 = 10.0 psia

P_E = 140.0 psia

γ = 1.395

T_1 = 519°R

T_E = 1250°R

Instrumentation and Associated Error:

1. Princo Fortin type barometer:	±0.005 psi
2. Doric DS-100 with Scannivalve & Statham 200 psig pressure transducer:	±0.10 psi
3. Doric DS-100 millivolt indicator:	±0.01% reading ±0.01% psi
4. Rosemount 414L bridge:	±0.1% reading ±0.03°F
5. Rosemount resistance thermometer:	±0.1% span or 0.25°C

Error Extremes in Measured Parameter:

$$P_1 = 10.0 \pm 0.105 \text{ psia}$$

$$P_E = 140.0 \pm 0.105 \text{ psia}$$

$$T_1 = 519°R \pm 1.00°R$$

$$T_E = 1250°R \pm 1.80°R$$

Calculation of Error Extremes in Efficiency:

Design Point

$$\eta = \frac{\left(\frac{140.0}{10}\right)^{\frac{0.395}{1.395}} - 1}{\frac{1250 - 519}{519}} = 0.79$$

Upper Limit With Error Maximized

$$\eta_{max} = \frac{\left(\frac{140.105}{9.895}\right)^{0.283} - 1}{\frac{1248.20 - 520.00}{520.00}} = 0.799$$

Lower Limit With Error Maximized

$$\eta_{min} = \frac{\left(\frac{139.895}{10.105}\right)^{0.283} - 1}{\frac{1251.80 - 518.00}{518.00}} = 0.78$$

Results

An approximation of error, assuming maximum error in instrumentation system, using the Doric Logging System with a Statham 200 psi pressure transducer and Rosemount platinum thermometer would indicate an uncertainity in computation of efficiency of ±1.0 from a design of 79.0.

The calculations do not take into account any errors caused by actual installation of sensors in the system. The system was calibrated prior to test, and all calibration corrections were applied. The system was operated at a stable ambient

temperature very near the conditions when calibrated. At 100 percent design speed, variation in inlet and exit discharge temperatures was of the order of 1.5 and 3.0°F respectively.

The computation of error should be used only as an approximation of limits anticipated using the described instrumentation system.

APPENDIX IV
CALIBRATION OF PRESSURE TRANSDUCER

MODEL: Statham PG-132TC-150-350

8th June, 1972
R. E. Kemp

SERIAL: 56493 CCN A150759

OPERATING CONDITIONS: 0 to 150 psig at -65 to +250°F. Installed in Scannivalve Model J. S/N 1005, CCN 101303.

DAS SETUP CONDITIONS: With no pressure applied, make the following adjustments to the Doric Digital Strain Gage Indicator.

1. Set excitation voltage to 5V, mV/sensitivity to 4.0, course span to 1.5, fine span to 0.06 and ride balance to +5.

2. Adjust fine bridge balance on the digital strain indicator to read 00.00 psi ± 0.01.

3. Depress the CAL button on front of the digital strain indicator. Adjust fine span until 116.05 ± 1 appears on the digital strain gage indicator.

4. Steps 2 and 3 should be repeated until both of the aforementioned readings are obtained on the Doric Digital Strain Gage indicator.

STANDARD USED:

Pressure gage, Heise	A150739
Manometer, Merriam	A150666

Applied Pressure PSIG at 75°F	Indicated Pressure PSIG
-3.50	-3.48
-3.00	-2.97
-2.50	-2.48
-2.00	-1.98
-1.50	-1.49
-1.00	-0.99
-0.50	-0.49
0.00	0.00

Applied Pressure PSIG at 75°F	Indicated Pressure PSIG
15.00	15.02
30.00	30.00
45.00	45.03
60.00	60.07
75.00	75.12
90.00	90.15
105.00	105.19
120.00	120.14
135.00	135.02
150.00	150.00

STATEMENT OF ACCURACY:

Within the operating and setup conditions stated above, pressure measurements at 75°F are estimated to be accurate with ± 0.10 psig. This accuracy applies only to the transducer-indicator system and does not include inherent errors of any pressure probes used.

APPENDIX V
COMPUTER PERFORMANCE LISTING, DATA POINT 44

The raw compressor performance data from the DAS printed paper listing provided the input data to program 440 "Two-Stage Compressor Performance." Typical transcribed computer output is listed in Tables VI, VII, and VIII for test data point 44 at 100% design speed.

The symbols used for the various compressor performance parameters are identified in the List of Symbols. Note that the computer printer output is limited to upper case symbols.

TABLE VI. COMPUTER EVALUATION OF TWO-STAGE COMPRESSOR PERFORMANCE

AMRDL TWO STAGE BUILD 1 TEST 06-28-72

REDUCED DATA

DATA POINT		44
N	RPM	83175.
W	PPS	1.3811
TUR. INLET PU1	PSI	74.83

FIRST STAGE

T1	DEG F	75.97
P TOT 1	PSIA	10.17
P STA 2	PSIA	29.64
P STA 3	PSIA	34.74
P STA 4	PSIA	43.76
P TOT E	PSIA	46.40
T2	DEG F	441.55

SECOND STAGE

T1	DEG F	441.55
P TOT 1	PSIA	46.40
P STA 2	PSIA	93.20
P STA 3	PSIA	105.12
P STA 4	PSIA	123.04
P STA E	PSIA	122.77
T2	DEG F	784.62

OVERALL

P STA OV	PSIA	122.77
T OVERALL	DEG F	784.62

TABLE VII. COMPUTER EVALUATION OF FIRST-STAGE PERFORMANCE

STAGE NO. 1 DATA POINT NO. 44

INDUCER STATION 1

LAMBDA 1	THETA 1	RHO 1	C1	PHI 1
1.00	0.0	0.04376	621.15	0.339

	HUB	RMS	SHROUD
DIA	1.440	2.595	3.375
U	522.60	941.64	1224.85
ALPHA 1	40.08	56.59	63.11
W1	811.75	1128.06	1373.34
M1W	0.737	1.025	1.248

IMPELLER TIP STATION 2

D2	B2	LAMBDA 2	U2	C2
5.050	0.29	0.95	1832.74	1263.24
W2	ALPHA 2	BETA 2	BETA 2*	M2
774.99	70.11	40.00	55.32	0.928
DEL Q DISC	Q	SLIP	RHO 2	W*SQR(T2)/P2
0.014	0.663	0.8069	0.10371	0.803
P2/P1	DF	OMEGA 1-2	U2/SQR(T1)	ETA 1-2
5.079	0.624	0.856	79.189	0.8561

DIFFUSER THROAT STATION 3

LAMBDA 3	A3	M3	DEL P 2-3/P2	CF 2-3
0.95	1.700	0.753	0.021	0.005
CP 2-3	W*SQR(T3)/P3	RWD	C2/C3	C3
0.232	0.820	0.943	1.2011	1051.71
P3/P1	ETA 1-3			
4.9735	0.8424			

VANED DIFFUSER STATION 4

LAMBDA 4	A4	M4	DEL P 3-4/P3	C4
0.840	3.280	0.3650	0.0514	530.346
C3/C4	CP 3-4	CP 2-4	P4/P1	ETA 1-4
1.983	0.570	0.642	4.7178	0.8081

COMPRESSOR EXIT STATION E

LAMBDA EXIT	ME	CE	DEL P 4-E/P4	CP 2-E
0.800	0.205	300.93	0.033	0.701

STAGE PERFORMANCE DATA

W*SQR(T1)/P1*A1	W*SQR(T1)/P1	W*SQR(THETA)/DEL	N/SQR(THETA)	U2/SQR(T1)
0.430	3.144	2.029	81873.19	79.189
PE TOT/P1	PE STA/P1	ETA 1-E TOT	ETA 1-E STA	(T2-T1)/T1
4.5634	4.4318	0.7868	0.7682	0.6825
Q	NS			
0.663	121.473			

TABLE VIII. COMPUTER EVALUATION OF SECOND-STAGE PERFORMANCE

STAGE NO. 2 DATA POINT NO. 44

INDUCER STATION 1

LAMBDA 1	THETA 1	RHO 1	C1	PHI 1
1.00	7.0	0.13217	447.85	0.260

	HUB	RMS	SHROUD
DIA	1.590	2.164	2.615
U	577.04	785.38	949.03
ALPHA 1	49.61	58.69	63.57
W1	685.97	855.37	998.82
M1W	0.470	0.586	0.685

IMPELLER TIP STATION 2

D2	B2	LAMBDA 2	U2	C2
4.752	0.180	0.95	1724.59	1238.07
W2	ALPHA 2	BETA 2	BETA 2*	M2
638.42	73.74	40.00	57.11	0.755
DEL Q DISC	Q	SLIP	RHO 2	W*SQR(T2)/P2
0.027	0.702	0.8290	0.22469	0.359
P2/P1	DF	OMEGA 1-2	U2/SQR(T1)	ETA 1-2
2.928	0.663	0.240	57.447	0.9338

DIFFUSER THROAT STATION 3

LAMBDA 3	A3	M3	DEL P 2-3/P2	CF 2-3
0.95	0.920	0.546	0.053	0.010
CP 2-3	W*SQR(T3)/P3	RWD	C2/C3	C3
0.280	0.379	0.792	1.3497	917.27
P3/P1	ETA 1-3			
2.7724	0.8793			

VANED DIFFUSER STATION 4

LAMBDA 4	A4	M4	DEL P 3-4/P3	C4
0.850	2.160	0.2272	0.0085	391.015
C3/C4	CP 3-4	CP 2-4	P4/P1	ETA 1-4
2.346	0.762	0.700	2.7487	0.8708

COMPRESSOR EXIT STATION E

LAMBDA EXIT	ME	CE	DEL P 4-E/P4	CP 2-E
0.800	0.171	295.20	0.018	0.694

STAGE PERFORMANCE DATA

W*SQR(T1)/P1*A1	W*SQR(T1)/P1	W*SQR(THETA)/DEL	N/SQR(THETA)	U2/SQR(T1)
0.264	0.894	0.577	623119.18	57.447
PE TOT/P1	PE STA/P1	ETA 1-E TOT	ETA 1-E STA	(T2-T1)/T1
2.7006	2.6461	0.8534	0.8333	0.3807
Q	NS			
0.702	72.790			

OVERALL PERFORMANCE DATA

P TOT OV/PT1	P STA OV/PT1	DEL T OV/T1	ETA OV T	ETA OV S
12.324	12.075	1.3230	0.7833	0.7745

FIRST STAGE W*SQR(T1)/P1*A1	FIRST STAGE W*SQR(T1)/P1	NET THRUST	FC1	FC2
0.430	3.144	95.00	221.22	108.80